Available online at http://scik.org
Commun. Math. Biol. Neurosci. 2026, 2026:31
https://doi.org/10.28919/cmbn/9716
ISSN: 2052-2541

MATHEMATICAL MODELING OF FILARIASIS AND HIV/AIDS CO-INFECTION IN THE CONTEXT OF VECTOR DYNAMICS

AMMA ACHIAA[1,*], EBENEZER BONYAH[2,3], ISAAC KWAME DONTWI[1], GASTON EDEM AWASHIE[1]

[1]Department of Mathematics, Kwame Nkrumah University of Science and Technology, Kumasi, Ghana

[2]Department of Mathematics Education, Akenten Appiah-Menka University of Skills Training and Entrepreneurial Development, Kumasi, Ghana

[3]Azerbaijan University of Architecture and Construction, 5 Ayna Sultanova Street, Baku AZ1073, Azerbaijan

Abstract. This study develops a unique fractional-order model comprising nine compartments to explore the dynamical behavior of the progression of filariasis and the immunosuppressive retrovirus (HIV) comorbidity under explicit vector influence. The study utilizes fractional order stochastic to examine the dynamics of randomness in the epidemiological model. Using fractional stability theory, we determined the reproduction number, the pathogen-absent state equilibrium, and the requirements for dual-level stability analytically. A center manifold approach is used to investigate bifurcation behavior at the critical threshold, demonstrating the forward bifurcation which the disease transmission can be early controlled by reducing R_0 less than zero. A fractional optimal control framework is developed; utilizing Pontryagin's Maximum Principle in the context of fractional order to provide the best strategy to manage the spread of the co-infection. We then did the numerical simulations to verify the theoretical findings and demonstrated how fractional stochastic models provide better understanding of the fluctuations in epdermiological models, and how fractional order can affect disease persistence and the effectiveness of combination therapies. According to our findings, in areas where HIV/AIDS and filariasis are endemic, memory effects play a crucial role in co-infection dynamics and provide guidance for developing integrated, economically sound public health programs. We also found out that, the strategic implementation of intense initial interventions

*Corresponding author
E-mail address: ammaachiaa095@gmail.com
Received November 28, 2025

is crucial in managing filariasis and HIV/AIDS co-infection. Thus, by prioritizing early intervention measures, the overall burden of the diseases would be significantly minimized. Therefore, the insights from our study will inform targeted interventions, optimize resource allocation, and improve the overall efficacy of public health strategies in regions burdened by multiple endemic diseases.

Keywords: filariasis; HIV; co-infection; fractional calculus; mathematical modeling; fractional optimal control.

2020 AMS Subject Classification: 92D30.

1. INTRODUCTION

HIV co-infection with filariasis is a complex public health problem, particularly in areas where both ailments are endemic [1]. Managing co-infections presents unique challenges due to the need for integrated treatment approaches that address both diseases simultaneously. This is complicated by the potential for drug interactions and the increased risk of adverse side effects. Additionally, co-infections can exacerbate the progression of each disease, making it more difficult to achieve successful health outcomes for affected individuals. Integrating biomedical, clinical, and mathematical modeling approaches is necessary for effective control and treatment options, as illustrated by immunological interactions and therapeutic outcomes.

According to [2] areas with high HIV incidence are frequently also areas with high LF prevalence, particularly in endemic regions across tropical Africa and southern Asia. This epidemiological convergence raises questions regarding co-infection dynamics, public health, and therapeutic interactions. HIV/AIDS depletes CD4+ T cells which will decrease the bodies' ability to cotrol the filarial worms. Filariasis causes a chronic immune activation leading to replication of the HIV virus which also welcomes more infections. It has been reported that filarial infections can alter the immune response of the host to HIV, leading to a The dominant profile of immunity [2].

About 40 million individuals are deformed and disabled, out of an estimated 120 million afflicted people globally, according to [3]. The fact that someone has HIV/ AIDS puts one at risk of infection because their immune system is very weak. Having a Filariasis co-infection makes the disease progression rapid compared to an individual without HIV/AIDS. The effectiveness of antiretroviral therapy (ART) may be diminished by filarial infections, which may also make an individual more susceptible to other opportunistic infections [2]. This is because filarial

parasites can alter immune responses, reducing the body's ability to control HIV replication [4]. Additionally, the presence of filarial infections may lead to increased inflammation, further exacerbating HIV-related complications and potentially reducing the overall effectiveness of ART in managing the disease. Due to its severity, there have been numerous studies which have explored the interaction between filarial infections and HIV, aiming to understand how these parasites influence immune function and disease outcomes [5, 6].

The co-infection of HIV/AIDS with filariasis results in intricate interactions that affect treatment efficacy as well as the course of the illness. A parasite infection spread by mosquitoes, filariasis mainly affects the lymphatic system, causing immunological modulation and chronic inflammation. HIV, on the other hand, depletes CD4 T-cells, which weakens the immune system. When both infections coexist, the persistent immunological activation brought on by filariasis might hasten HIV replication and the development of AIDS, while the immune suppression brought on by HIV increases the persistence and intensity of filarial parasites. Both diseases' natural course is altered by this reciprocal interaction, which also makes therapeutic care more difficult [7, 8].

From an epidemiological perspective, areas with high HIV prevalence and filariasis-endemic zones overlap, especially in sub-Saharan Africa, which raises the possibility of co-infection within afflicted people. By affecting susceptibility and infectiousness, the interactions between the two pathogens might alter the dynamics of transmission. For instance, whereas HIV-induced immunosuppression might prolong the existence of microfilariae in the circulation, boosting vector infection rates, filarial infection may raise HIV viral load and enhance transmission potential. As a result, by maintaining dual transmission cycles, the co-infection not only affects individual health outcomes but also presents more significant public health issues [9, 10].

A useful foundation for comprehending these coupled dynamics and creating efficient control measures is provided by mathematical modeling of filariasis–HIV co-infection. In example, fractional-order models have been used to describe illness progression more accurately by capturing the memory and genetic characteristics inherent in biological systems. These models include human and vector compartments, emphasizing the impact of immune response, treatment, and prevention on the spread of both diseases. These models identify crucial thresholds, such as

the fundamental reproduction number, that control the co-infection's persistence or eradication through numerical simulations and bifurcation analysis. In order to achieve sustainable disease control, insights from these analyses help build integrated intervention plans that address both diseases at the same time [11, 12].

Mathematical modeling has evolved into an indispensable framework for analyzing infectious disease transmission and informing public health policy. Mathematical modeling is widely used to analyze the interplay between co-infecting pathogens and their influence on the host immune response. For example, the studies of [13] introduced a quantitative model capturing the synergistic transmission between two interacting pathogens, highlighting the complex dynamics of co-infection. [14] Provides a comprehensive analysis of dengue fever dynamics within a mathematical construct that embeds awareness. [15], formulated a mathematical model to examine the interactive transmission patterns between malaria and COVID-19 infections. Also, [16] formulated a mathematical framework to explore the interaction between malaria and cholera co-infections. This highlighted malaria's influence on cholera dynamics. These models help identify key factors that influence co-infection outcomes, supporting the development of targeted interventions to improve patient health and treatment efficacy. These models also provide insights into how co-infections interact and influence each other's progression. By identifying critical parameters, such as transmission rates and immune responses, researchers can develop more effective strategies for managing and preventing co-infections, ultimately improving public health outcomes.

In recent decades, fractional calculus has gained prominence as a compelling framework for modeling real-world phenomena, owing to its intrinsic memory properties, which offer greater flexibility than classical integer-order formulations [17, 18, 19]. Fractional calculus, a generalization of traditional calculus, offer fractional-order formulations analytical platform capable of capturing the memory-driven and hereditary mechanisms that govern complex epidemic dynamics. By incorporating derivatives and integrals of non-integer orders, it enables a more nuanced understanding of complex biological interactions. It enhances the accuracy of predictive models, revealing subtle dynamics that standard calculus might overlook. as such most studies on coinfections have focused on the incorporation of fractional calculus to model the dynamics

of co-infections, emphasizing the interplay between immune responses and pathogen behavior. The studies of [20] presented a fractional-order model for analyzing malaria and COVID-19 co-infections, highlighting disease stages and model stability. [21] examined the interplay between malaria and HIV co-infection using a delay fractional order model. [22] developed a fractional model describing the co-infection dynamics of HBV and HCV, employing the Mittag-Leffler derivative and fixed point theory for the analysis.

Relying on these studies, we present a mathematical model based on fractional-order dynamics that explores the transmission dynamics of filariasis and HIV/AIDS to guide the progression of the disease dynamics from an undesirable endemic state toward a targeted controlled outcome. We contribute to literature by highlighting the interaction between the two infections and their shared impact on the health of the population. By incorporating fractional calculus, our model captures the memory-dependent nature of disease transmission, offering a more realistic representation of the dynamics. Thus providing valuable insights for designing effective control strategies. Our work bridges a gap in existing literature by incorporating a more accurate representation of the time-dependent behavior of disease transmission. By employing fractional-order calculus, the model accounts for memory and non-local effects dynamics, which are often overlooked in traditional integer-order models, enhancing the predictive accuracy and providing deeper insights into the interplay between filariasis and HIV/AIDS. Thus, our study seeks to identify strategies that maximize public health benefits while minimizing economic costs to provide policymakers with actionable insights for implementing efficient disease management programs.

2. PRELIMINARIES

2.1. Mathematical Model Formulation. In this section, a filariasis–HIV/AIDS co-infection mathematical model is presented in which the total human population, $N_h(t)$, is partitioned into the following compartments: susceptible individuals (S_h), individuals infected with filariasis (I_f), HIV-positive individuals (I_h), HIV-infected individuals under management or treatment (I_m), co-infected individuals with both filariasis and HIV (I_{fh}), treated co-infected individuals (T_{fh}), and individuals who have recovered from filariasis (R_f). The mosquito (vector) population, $N_v(t)$, is categorized into susceptible mosquitoes (S_v) and infected vector insects (I_v).

2.2. Model Diagram.

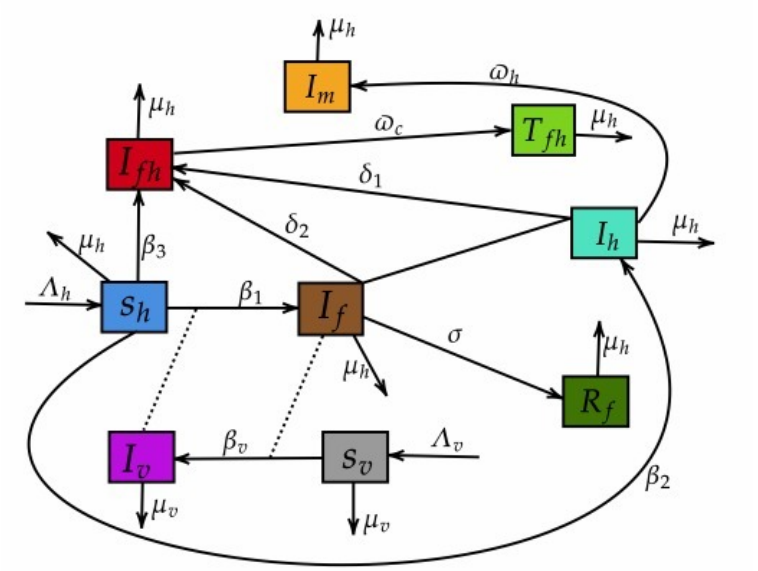

FIGURE 1. Model flow diagram

Parameter	Description
Λ_h	Recruitment rates of humans
Λ_v	Recruitment rates of vectors
β_1	Transmission rates for filariasis
β_2	Transmission rates for HIV
β_3	Transmission rates for co-infection
β_4	Transmission rates for vectors
δ_1, δ_2	Enhancement factors for co-infection dynamics
σ	Recovery rate from filariasis
ϖ_h	Transmission rates to managed HIV
ϖ_c	Transmission rates to managed co-infection
μ_h	Natural death rates of humans
μ_v	Natural death rates of vectors

TABLE 1. Parameter descriptions for the filariasis–HIV/AIDS co-infection model.

2.3. Model Equations.

$$
\begin{aligned}
\frac{dS_h}{dt} &= \Lambda_h - \beta_1 S_h I_v - \beta_2 S_h I_h - \beta_3 S_h I_{fh} - \mu_h S_h,\\
\frac{dI_f}{dt} &= \beta_1 S_h I_v - \delta_2 I_f I_h - (\sigma + \mu_h) I_f,\\
\frac{dI_h}{dt} &= \beta_2 S_h I_h - \delta_1 I_f I_h - (\varpi_h + \mu_h) I_h,\\
\frac{dI_m}{dt} &= \varpi_h I_h - \mu_h I_m,\\
\frac{dI_{fh}}{dt} &= \beta_3 S_h I_{fh} + \delta_1 I_f I_h + \delta_2 I_f I_h - (\varpi_c + \mu_h) I_{fh},\\
\frac{dT_{fh}}{dt} &= \varpi_c I_{fh} - \mu_h T_{fh},\\
\frac{dR_f}{dt} &= \sigma I_f - \mu_h R_f,\\
\frac{dS_v}{dt} &= \Lambda_v - \beta_v S_v I_f - \mu_v S_v,\\
\frac{dI_v}{dt} &= \beta_v S_v I_f - \mu_v I_v.
\end{aligned}
\tag{1}
$$

.

3. Main Results

3.1. Model analysis.

3.1.1. *Well Posedness of the model.* To prove the well posedness of our model, we express system 1 into the form:

$$
\frac{dW}{dt} = F(W), \tag{2}
$$

where $W = (S_h, I_f, I_h, I_m, I_f h, T_f h, R_f, S_v, I_v) \in \mathbb{R}^9$, and

$$F(W) = \begin{pmatrix} \Lambda_h - \beta_1 S_h I_v - \beta_2 S_h I_h - \beta_3 S_h I_f h - \mu_h S_h \\ \beta_1 S_h I_v - \sigma I_f - \delta_1 I_f I_h - \mu_h I_f \\ \beta_2 S_h I_h - \delta_2 I_h I_f - \mu_h I_h - \varpi_h I_h \\ \varpi_h I_h - \mu_h I_m \\ \beta_3 S_h I_f h + \delta_2 I_f I_h + \delta_1 I_h I_f - \mu_h I_f h - \varpi_c I_f h \\ \varpi_c I_f h - \mu_h T_f h \\ \sigma I_f - \mu_h R_f \\ \Lambda_v - \beta_v S_v I_f - \mu_v S_v \\ \beta_v S_v I_f - \mu_v I_v \end{pmatrix} \tag{3}$$

subject to the initial condition $W(0) = W_0 = (S_{h0}, I_{f0}, I_{h0}, I_{m0}, I_{fh0}, T_{fh0}, R_{f0}, S_{v0}, I_{v0}) \in \mathbb{R}^9_{\geq 0}$.

Theorem 1 Picard-Lindelöf Theorem [23]: For $\frac{dW}{dt} = F(W)$, where $W(0) = W_0$, a single solution exists on the interval $[0, T]$ provided that:

- $W \in D \subset \mathbb{R}^9$ with $W_0 \in D$;
- $F(W)$ is continuous on W.
- $F(W)$ satisfies the Lipschitz condition in D; that is, there exists a constant $L > 0$ such that for all $W, Y \in D$, $\|F(W) - F(Y)\| \leq L\|W - Y\|$

Proof:

We consider a compact domain:

$$D = [0, K]^9 = \{(S_h, I_f, I_h, I_m, I_f h, T_f h, R_f, S_v, I_v) \mid 0 \leq S_h, I_f, I_h, I_m, I_f h, T_f h, R_f, S_v, I_v \leq K\},$$

The constant $K > 0$ is taken to include W_0 and to represent biologically admissible values. Given that $F(W)$ is a polynomial function of the state variables: $S_h, I_f, I_h, I_m, I_f h, T_f h, R_f, S_v, I_v$ with constant coefficients, it is continuous in W for all $W \in \mathbb{R}^9$. Thus, $F(W)$ is continuous in the compact domain $D = [0, K]^9$.

Lipschitz Continuity of $F(W)$. To verify Lipschitz continuity, we consider the Jacobian matrix $J(W)$ of $F(W)$ in D, which is the matrix of partial derivatives $(\partial f_i)/\partial w_j$, where $w_1 = S_h$,

$w_2 = I_f$, $w_3 = I_h$, $w_4 = I_m$, $w_5 = I_f h$, $w_6 = T_f h$, $w_7 = R_f$, $w_8 = S_v$, $w_9 = I_v$

$$J(W) = \begin{pmatrix} -\beta_1 I_v - \beta_2 I_h - \beta_3 I_{fh} - \mu_h & 0 & -\beta_2 S_h & 0 & -\beta_3 S_h & 0 & 0 & 0 & -\beta_1 S_h \\ \beta_1 I_v & -(\sigma + \delta_1 I_h + \mu_h) & -\delta_1 I_f & 0 & 0 & 0 & 0 & 0 & \beta_1 S_h \\ \beta_2 I_h & -\delta_2 I_f & \beta_2 S_h - \delta_2 I_h - \mu_h - \varpi_h & 0 & 0 & 0 & 0 & 0 & 0 \\ 0 & 0 & \varpi_h & -\mu_h & 0 & 0 & 0 & 0 & 0 \\ \beta_3 I_{fh} & I_h(\delta_1 + \delta_2) & I_f(\delta_1 + \delta_2) & 0 & \beta_3 S_h - \mu_h - \varpi_c & 0 & 0 & 0 & 0 \\ 0 & 0 & 0 & 0 & \varpi_c & -\mu_h & 0 & 0 & 0 \\ 0 & \sigma & 0 & 0 & 0 & 0 & -\mu_h & 0 & 0 \\ 0 & -\beta_v S_v & 0 & 0 & 0 & 0 & 0 & -\beta_v I_f - \mu_v & 0 \\ 0 & \beta_v S_v & 0 & 0 & 0 & 0 & 0 & 0 & -\mu_v \end{pmatrix}$$

In the compact domain $D = [0,K]^9$, the non-zero entries of $J(W)$ are bounded as follows:

$$\left|-(\beta_1 I_v - \beta_2 S_h - \beta_3 I_f h - \mu_h)\right| \leq \beta_1 K + \beta_2 K + \beta_3 K + \mu_h,$$

$$\left|\pm\beta_1 S_h I_v\right|, \left|\pm\beta_1 S_h I_h\right|, \left|\beta_3 S_h I_f h\right| \leq (\beta_1 K)^2$$

Constants like $\sigma, \mu_h, \varpi_h, \mu_v$ are fixed. Using the infinity norm (maximum row sum of $|J(W)|$), we compute the bounds for each row and obtain the Lipschitz constant as: $L = \max\Big\{2(\beta_1 + \beta_2 + \beta_3)K + \mu_h, 2\beta_1 K + \sigma + 2\delta_1 K + \mu_h, 2\beta_2 K + 2\delta_2 K + \mu_h + \varpi_h, \varpi_h + \mu_h, 2\beta_3 K + 2(\delta_1 + \delta_2)K + \mu_h + \varpi_c, \varpi_c + \mu_h, \sigma + \mu_h, \beta_v K + \mu_v\Big\}$ which is finite for $K < \infty$, confirming $F(W)$ is Lipschitz continuous in D. Since $F(W)$ is continuous (as a polynomial) and Lipschitz continuous in D, the Picard-Lindelöf theorem ensures the existence of a single solution on the interval $[0,T]$ for any $W_0 \in D$. Thus, the solution exists uniquely for all $t \geq 0$.

3.1.2. *Positivity Analysis.* We demonstrate that all state variables $S_h, I_f, I_h, I_m, I_f h, T_f h, R_f, S_v, I_v$ remain non-negative for all $t \geq 0$ under non-negative initial conditions $W(0) = (S_{h0}, I_{f0}, I_{h0}, I_{m0}, I_{fh0}, T_{fh0}, R_{f0}, S_{v0}, I_{v0}) \in \mathbb{R}^9_{\geq 0}$ where all model parameters are non-negative. For each State Variable:

- S_h: The derivative is $\frac{dS_h}{dt} = \Lambda_h - (\beta_1 I_v + \beta_2 I_h + \beta_3 I_f h + \mu_h)S_h$. If $S_h = 0$, $\frac{dS_h}{dt} = \Lambda_h \geq 0$, maintaining or increasing S_h. For $S_h > 0$, the solution remains positive.
- I_f: The derivative is $\frac{dI_f}{dt} = \beta_1 S_h I_v - (\sigma + \delta_1 I_h + \mu_h)I_f$. If $I_f = 0$, $\frac{dI_f}{dt} = \beta_1 S_h I_v \geq 0$, keeping $I_f \geq 0$.

- I_h: The derivative is $\frac{dI_h}{dt} = \beta_2 S_h I_h - (\delta_2 I_f + \mu_h + \varpi_h) I_h$. If $I_h = 0$, $\frac{dI_h}{dt} = 0$, preserving $I_h \geq 0$.
- I_m: The derivative is $\frac{dI_m}{dt} = \varpi_h I_h - \mu_h I_m$. If $I_m = 0$, $\frac{dI_m}{dt} = \varpi_h I_h \geq 0$, ensuring $I_m \geq 0$.
- $I_f h$: The derivative is $\frac{dI_{fh}}{dt} = (\beta_3 S_h I_f h + \delta_1 I_f I_h + \delta_2 I_h I_f) - (\mu_h + \varpi_c) I_f h$. If $I_f h = 0$, $\frac{dI_{fh}}{dt} = \beta_3 S_h I_v + \delta_1 I_f I_h + \delta_2 I_h I_f \geq 0$, keeping $I_f h \geq 0$.
- $T_f h$: The derivative is $\frac{dT_{fh}}{dt} = \varpi_c I_f h - \mu_h T_f h$. If $T_f h = 0$, $\frac{dT_{fh}}{dt} = \varpi_c I_f h \geq 0$, ensuring $T_f h \geq 0$.
- R_f: The derivative is $\frac{dR_f}{dt} R_f = \sigma I_f - \mu_h R_f$. If $R_f = 0$, $\frac{dR_f}{dt} = \sigma I_f \geq 0$, keeping $R_f \geq 0$.
- S_v: The derivative is $\frac{dS_v}{dt} = \Lambda_v + (\mu_v - \beta_v I_f) S_v$. If $S_v = 0$, $\frac{dS_v}{dt} = \Lambda_v \geq 0$, maintaining or increasing S_v.
- I_v: The derivative is $\frac{dI_v}{dt} = \beta_v S_v I_f - \mu_v I_v$. If $I_v = 0$, $\frac{dI_v}{dt} = \beta_v S_v I_f \geq 0$, ensuring $I_v \geq 0$.

The system $\frac{dW}{dt} = F(W)$ ensures that the derivative of each component is non-negative when the component is zero, provided the other variables are non-negative, due to non-negative source terms (Λ_h and other parameters). The continuity and Lipschitz continuity of $F(W)$ (established earlier) ensure smooth evolution, and the Picard-Lindelöf theorem guarantees a unique solution that remains in $\mathbb{R}^9_{\geq 0}$ starting from non-negative initial conditions. It follows that all state variables stay non-negative for every $t \geq 0$ under non-negative initial conditions.

3.1.3. *Boundedness and Finiteness of the Model.* To show that the model is bounded and finite, we analyze the entire human population $N_h = S_h + I_f + I_h + I_m + I_f h + T_f h + R_f$ and the entire vector population $N_v = S_v + I_v$. For the total human population we compute the time derivative and obtain:

$$\frac{dN_h}{dt} = \Lambda_h - \mu_h (S_h + I_f + I_h + I_m + I_f h + T_f h + R_f) = \Lambda_h - \mu_h N_h. \tag{4}$$

The solution of 4, assuming $\mu_h > 0$, is:

$$N_h(t) = N_h(0) e^{-\mu_h t} + \frac{\Lambda_h}{\mu_h} (1 - e^{-\mu_h t}). \tag{5}$$

As $t \to \infty$, $N_h(t) \to \Lambda_h / \mu_h$. Given that the initial conditions are non-negative, $N_h(0) \geq 0$, $N_h(t) \leq \max(N_h(0), \Lambda_h / \mu_h)$. Thus, N_h is bounded above by the finite value Λ_h / μ_h. For the

total Mosquito Population, we compute the time derivative and obtain:

$$\frac{dN_v}{dt} = [\Lambda_v - \beta_v S_v(I_f + I_f h) - \mu_v S_v] + [\beta_v S_v(I_f + I_f h) - \mu_v I_v]. \tag{6}$$

The solution 6, assuming $\mu_v > 0$, is:

$$N_v(t) = N_v(0)e^{-\mu_v t} + \frac{\Lambda_v}{\mu_v}(1 - e^{-\mu_v t}). \tag{7}$$

As $t \to \infty$, $N_v(t) \to \Lambda_v/\mu_v$. With non-negative initial conditions $N_v(0) \geq 0$, $N_v(t) \leq \max(N_v(0), \Lambda_v/\mu_v)$. Thus, N_v is bounded above by the finite value Λ_v/μ_v. Each state variable $(S_h, I_f, I_h, I_m, I_f h, T_f h, R_f, S_v, I_v)$ is non-negative. Since N_h and N_v are bounded, the individual components are also bounded. Hence, the model is bounded and finite because: The total populations N_h and N_v approach finite steady-state values Λ_h/μ_h and Λ_v/μ_v, respectively, under the condition that $\mu_h, \mu_v > 0$.

3.2. Equilibrium Analysis.

3.2.1. *Disease-Free Equilibrium (DFE).* To determine the disease-free equilibrium, all infected compartments are set to zero ($I_f = 0$, $I_h = 0$, $I_m = 0$, $I_f h = 0$, $T_f h = 0$, $I_v = 0$) and solve for the non-infected compartments S_h, R_f, S_v. Therefore, the disease-free equilibrium is given by:

$$E_0 = \left(\frac{\Lambda_h}{\mu_h}, 0, 0, 0, 0, 0, 0, \frac{\Lambda_v}{\mu_v}, 0\right). \tag{8}$$

3.2.2. *Endemic Equilibrium.* To analyze the endemic equilibrium of the model, all time derivatives are equated to zero, and the resulting system of algebraic equations is solved accordingly. Therefore, the endemic equilibrium point can be expressed as:

$$S_v^* = \frac{\Lambda_v}{A}, \quad I_v^* = \frac{I_f^* \Lambda_v \beta_v}{\mu_v A}, \quad I_f h^* = \frac{F}{\mu_h + \varpi_c},$$

$$S_h^* = \frac{\Lambda_h}{\mu_h + I_h^* \beta_2 + \left(\frac{\beta_3 F}{\mu_h + \varpi_c} + C\right)},$$

$$I_m^* = \frac{I_h^* \varpi_h}{\mu_h}, \quad T_f h^* = \frac{\varpi_c F}{\mu_h(\mu_h + \varpi_c)}, \quad R_f^* = \frac{I_f^* \sigma}{\mu_h}.$$

with auxiliary variables:

$$A = \mu_v + I_f^* \beta_v, \quad B = \mu_v A, \quad C = \frac{I_f^* \Lambda_v \beta_1 \beta_v}{B},$$

$$D = \mu_h + I_f h^* \beta_3 + I_h^* \beta_2 + C = \mu_h + \frac{F\beta_3}{\mu_h + \varpi_c} + I_h^* \beta_2 + C,$$

$$E = \frac{I_f^* \Lambda_h \Lambda_v \beta_3 \beta_v}{BD}, \quad F = I_f^* I_h^* (\delta_1 + \delta_2) + E.$$

3.2.3. *Basic Reproduction Number (R_0).* The basic reproduction number (R_0) is determined through the application of the next-generation matrix approach, based on the model equations and evaluated at the disease-free equilibrium point (DFE). The susceptible populations at the DFE are $N_h = \Lambda_h/\mu_h$ and $N_v = \Lambda_v/\mu_v$.

Next-Generation Matrix Method. Infected compartments: $I_f, I_h, I_m, I_{fh}, I_v$. New infections:

$$\mathscr{F} = \begin{pmatrix} \beta_1 S_h I_v \\ \beta_2 S_h I_h \\ 0 \\ \beta_3 S_h I_{fh} \\ \beta_v S_v I_f \end{pmatrix}$$

Transitions:

$$\mathscr{V} = \begin{pmatrix} \sigma I_f + \delta_1 I_f I_h + \mu_h I_f \\ \delta_2 I_h I_f + \mu_h I_h + \varpi_h I_h \\ \varpi_h I_h + \mu_h I_m \\ \delta_1 I_f I_h + \delta_2 I_h I_f + \mu_h I_{fh} + \varpi_c I_{fh} \\ \mu_v I_v \end{pmatrix}$$

At the DFE, the matrices are:

$$F = \begin{pmatrix} 0 & 0 & 0 & 0 & \beta_1 \frac{\Lambda_h}{\mu_h} \\ 0 & \beta_2 \frac{\Lambda_h}{\mu_h} & 0 & 0 & 0 \\ 0 & 0 & 0 & 0 & 0 \\ 0 & 0 & 0 & \beta_3 \frac{\Lambda_h}{\mu_h} & 0 \\ \beta_v \frac{\Lambda_v}{\mu_v} & 0 & 0 & 0 & 0 \end{pmatrix},$$

$$V = \begin{pmatrix} -(\sigma+\mu_h) & 0 & 0 & 0 & 0 \\ 0 & -(\mu_h+\varpi_h) & 0 & 0 & 0 \\ 0 & \varpi_h & -\mu_h & 0 & 0 \\ 0 & 0 & 0 & -(\mu_h+\varpi_c) & 0 \\ 0 & 0 & 0 & 0 & -\mu_v \end{pmatrix},$$

$$V^{-1} = \begin{pmatrix} \frac{1}{\sigma+\mu_h} & 0 & 0 & 0 & 0 \\ 0 & \frac{1}{\mu_h+\varpi_h} & 0 & 0 & 0 \\ 0 & \frac{\varpi_h}{\mu_h(\mu_h+\varpi_h)} & \frac{1}{\mu_h} & 0 & 0 \\ 0 & 0 & 0 & \frac{1}{\mu_h+\varpi_c} & 0 \\ 0 & 0 & 0 & 0 & \frac{1}{\mu_v} \end{pmatrix},$$

$$FV^{-1} = \begin{pmatrix} 0 & 0 & 0 & 0 & \frac{\beta_1\Lambda_h}{\mu_h\mu_v} \\ 0 & \frac{\beta_2\Lambda_h}{\mu_h(\mu_h+\varpi_h)} & \frac{\beta_2\Lambda_h\varpi_h}{{\mu_h}^2(\mu_h+\varpi_h)} & 0 & 0 \\ 0 & 0 & 0 & 0 & 0 \\ 0 & 0 & 0 & \frac{\beta_3\Lambda_h}{\mu_h(\mu_h+\varpi_c)} & 0 \\ \frac{\beta_v\Lambda_v}{\mu_v(\sigma+\mu_h)} & 0 & 0 & 0 & 0 \end{pmatrix}.$$

The spectral radius is:

$$\rho(FV^{-1}) = R_0 = \sqrt{\frac{\beta_1\beta_v\Lambda_h\Lambda_v}{(\sigma+\mu_h)\mu_h{\mu_v}^2}}.$$

Thus,

$$R_0 = \sqrt{\frac{\beta_1\beta_v\Lambda_h\Lambda_v}{(\sigma+\mu_h)\mu_h{\mu_v}^2}}. \tag{9}$$

3.3. Stability Analysis.

3.3.1. *Local Stability Analysis of the Disease-Free Equilibrium.* To determine the local stability of 8 of the given system 1, we compute the Jacobian matrix, evaluate it at the DFE E_0^{fh},

and analyze its eigenvalues. Thus, we obtain:

(10)
$$J(E_0) = \begin{pmatrix} -\mu_h & 0 & -\beta_2\frac{\Lambda_h}{\mu_h} & 0 & -\beta_3\frac{\Lambda_h}{\mu_h} & 0 & 0 & 0 & -\beta_1\frac{\Lambda_h}{\mu_h} \\ 0 & -\sigma-\mu_h & 0 & 0 & 0 & 0 & 0 & 0 & \beta_1\frac{\Lambda_h}{\mu_h} \\ 0 & 0 & \beta_2\frac{\Lambda_h}{\mu_h}-\mu_h-\varpi_h & 0 & 0 & 0 & 0 & 0 & 0 \\ 0 & 0 & \varpi_h & -\mu_h & 0 & 0 & 0 & 0 & 0 \\ 0 & 0 & 0 & 0 & \beta_3\frac{\Lambda_h}{\mu_h}-\mu_h-\varpi_c & 0 & 0 & 0 & 0 \\ 0 & 0 & 0 & 0 & \varpi_c & -\mu_h & 0 & 0 & 0 \\ 0 & -\sigma & 0 & 0 & 0 & 0 & -\mu_h & 0 & 0 \\ 0 & -\beta_v\frac{\Lambda_v}{\mu_v} & 0 & 0 & 0 & 0 & 0 & -\mu_v & 0 \\ 0 & \beta_v\frac{\Lambda_v}{\mu_v} & 0 & 0 & 0 & 0 & 0 & 0 & -\mu_v \end{pmatrix}.$$

From 10, the diagonal eigenvalues are:

- $\lambda_1 = -\mu_h < 0$,
- $\lambda_2 = -\sigma - \mu_h < 0$,
- $\lambda_3 = \beta_2\frac{\Lambda_h}{\mu_h} - \mu_h - \varpi_h < 0$ if $\beta_2\frac{\Lambda_h}{\mu_h} \leq 0$ (which holds at DFE),
- $\lambda_4 = -\mu_h < 0$,
- $\lambda_5 = \beta_3\frac{\Lambda_h}{\mu_h} - \mu_h - \varpi_c < 0$ if $\beta_3\frac{\Lambda_h}{\mu_h} \leq 0$ (which holds at DFE),
- $\lambda_6 = -\mu_h < 0$,
- $\lambda_7 = -\mu_h < 0$,
- $\lambda_8 = -\mu_v < 0$,
- $\lambda_9 = -\mu_v < 0$.

The only potentially non-negative eigenvalue comes from the infected subsystem involving I_f and I_v, which is controlled by R_0. Hence, the DFE is locally asymptotically stable if

$$R_0 = \sqrt{\frac{\beta_1\beta_v\Lambda_h\Lambda_v}{(\sigma+\mu_h)\mu_h{\mu_v}^2}} < 1.$$

3.3.2. *Local Stability Analysis of the Endemic Equilibrium.* We analyze the local stability of the endemic equilibrium for a 9-dimensional HIV-filariasis co-infection transmission model. The endemic equilibrium is:

$$S_v^* = \frac{\Lambda_v}{A}, \quad I_v^* = \frac{I_f^*\Lambda_v\beta_v}{\mu_v A}, \quad I_{fh}^* = \frac{F}{\mu_h+\varpi_c},$$

$$S_h^* = \frac{\Lambda_h}{\mu_h + I_h^*\beta_2 + \left(\frac{\beta_3 F}{\mu_h+\varpi_c} + C\right)}, \quad I_m^* = \frac{I_h^*\varpi_h}{\mu_h},$$

$$T_{fh}^* = \frac{\varpi_c F}{\mu_h(\mu_h+\varpi_c)}, \quad R_f^* = \frac{I_f^*\sigma}{\mu_h}.$$

with auxiliary variables:

$$A = \mu_v + I_f^*\beta_v, \quad B = \mu_v A, \quad C = \frac{I_f^*\Lambda_v\beta_1\beta_v}{B},$$

$$D = \mu_h + I_{fh}^*\beta_3 + I_h^*\beta_2 + C = \mu_h + \frac{F\beta_3}{\mu_h+\varpi_c} + I_h^*\beta_2 + C,$$

$$E = \frac{I_f^*\Lambda_h\Lambda_v\beta_3\beta_v}{BD}, \quad F = I_f^*I_h^*(\delta_1+\delta_2) + E.$$

The equilibrium depends on $I_f^* > 0$, $I_h^* > 0$, which are not explicitly solved due to nonlinearities. We assume a valid endemic equilibrium exists. To determine local stability, we compute the Jacobian matrix, evaluate it at the endemic equilibrium, and analyze its eigenvalues. The equilibrium is locally asymptotically stable if all eigenvalues have negative real parts. The Jacobian at the endemic equilibrium is:

$$J_{ee}^* = \begin{pmatrix}
-\left(\beta_1\frac{I_f^*\Lambda_v\beta_v}{\mu_v A} + \beta_2 I_h^* + \beta_3\frac{F}{\mu_h+\varpi_c} + \mu_h\right) & 0 & -\beta_2 S_h^* & 0 & -\beta_3 S_h^* & 0 & 0 & 0 & -\beta_1 S_h^* \\
\beta_1\frac{I_f^*\Lambda_v\beta_v}{\mu_v A} & -(\sigma+\delta_1 I_h^*+\mu_h) & -\delta_1 I_f^* & 0 & 0 & 0 & 0 & 0 & \beta_1 S_h^* \\
\beta_2 I_h^* & -\delta_2 I_f^* & \beta_2 S_h^* - \delta_2 I_h^* - \mu_h - \varpi_h & 0 & 0 & 0 & 0 & 0 & 0 \\
0 & 0 & \varpi_h & -\mu_h & 0 & 0 & 0 & 0 & 0 \\
\beta_3\frac{F}{\mu_h+\varpi_c} & (\delta_1+\delta_2)I_h^* & (\delta_1+\delta_2)I_f^* & 0 & \beta_3 S_h^* - \mu_h - \varpi_c & 0 & 0 & 0 & 0 \\
0 & 0 & 0 & 0 & \varpi_c & -\mu_h & 0 & 0 & 0 \\
0 & \sigma & 0 & 0 & 0 & 0 & -\mu_h & 0 & 0 \\
0 & -\beta_v\frac{\Lambda_v}{\mu_v} & 0 & 0 & 0 & 0 & 0 & -\beta_v I_f^* - \mu_v & 0 \\
0 & \beta_v\frac{\Lambda_v}{\mu_v} & 0 & 0 & 0 & 0 & 0 & \beta_v I_f^* & -\mu_v
\end{pmatrix}$$

The equilibrium is considered stable when all the eigenvalues of J_{ee}^* possess negative real parts. The diagonal entries $J_{44} = J_{66} = J_{77} = -\mu_h$ yield three eigenvalues:

$$\lambda_4 = \lambda_6 = \lambda_7 = -\mu_h < 0,$$

These correspond to the decoupled dynamics of I_m, T_{fh}, and R_f, which are stable. The remaining 6×6 submatrix will be analyzed for $(S_h, I_f, I_h, I_{fh}, S_v, I_v)$:

$$J^*_{ee(\text{reduced})} = \begin{pmatrix} -\left(\beta_1 \frac{I_f^*\Lambda_v\beta_v}{\mu_v A} + \beta_2 I_h^* + \beta_3 \frac{F}{\mu_h+\varpi_c} + \mu_h\right) & 0 & -\beta_2 S_h^* & -\beta_3 S_h^* & 0 & -\beta_1 S_h^* \\ \beta_1 \frac{I_f^*\Lambda_v\beta_v}{\mu_v A} & -(\sigma+\delta_1 I_h^* + \mu_h) & -\delta_1 I_f^* & 0 & 0 & \beta_1 S_h^* \\ \beta_2 I_h^* & -\delta_2 I_f^* & \beta_2 S_h^* - \delta_1 I_h^* - \mu_h - \varpi_h & 0 & 0 & 0 \\ \beta_3 \frac{F}{\mu_h+\varpi_c} & (\delta_1+\delta_2) I_h^* & (\delta_1+\delta_2) I_f^* & \beta_3 S_h^* - \mu_h - \varpi_c & 0 & 0 \\ 0 & -\beta_v \frac{\Lambda_v}{\mu_v} & 0 & 0 & -\beta_v S_v^* - \mu_v & 0 \\ 0 & \beta_v \frac{\Lambda_v}{\mu_v} & 0 & 0 & \beta_v S_v^* & -\mu_v \end{pmatrix} \tag{12}$$

Block Decomposition. The sub-matrix has a block structure:

Human block (S_h, I_f, I_h, I_{fh}):

(11)

$$J^*_{ee(\text{human})} = \begin{pmatrix} -(\beta_1 \frac{I_f^*\Lambda_v\beta_v}{\mu_v A} + \beta_2 I_h^* + \beta_3 \frac{F}{\mu_h+\varpi_c} + \mu_h) & 0 & -\beta_2 S_h^* & -\beta_3 S_h^* \\ \beta_1 \frac{I_f^*\Lambda_v\beta_v}{\mu_v A} & -(\sigma+\delta_1 I_h^* + \mu_h) & -\delta_1 I_f^* & 0 \\ \beta_2 I_h^* & -\delta_2 I_f^* & \beta_2 S_h^* - \delta_1 I_h^* - \mu_h - \varpi_h & 0 \\ \beta_3 \frac{F}{\mu_h+\varpi_c} & (\delta_1+\delta_2) I_h^* & (\delta_1+\delta_2) I_f^* & \beta_3 S_h^* - \mu_h - \varpi_c \end{pmatrix}.$$

Vector block (S_v, I_v):

(12)
$$J^*_{ee(\text{vector})} = \begin{pmatrix} -\beta_v I_f^* - \mu_v & 0 \\ \beta_v I_f^* & -\mu_v \end{pmatrix}.$$

Vector Block Eigenvalues: Computing the characteristic polynomial of J_{vector}:

$$\det(\lambda I - J_{\text{vector}}) = \det\begin{pmatrix} \beta_v I_f^* + \mu_v + \lambda & 0 \\ -\beta_v I_f^* & \lambda + \mu_v \end{pmatrix} = (\beta_v I_f^* + \mu_v + \lambda)(\lambda + \mu_v) = 0,$$

$$\lambda_8 = -\beta_v I_f^* - \mu_v < 0, \quad \lambda_9 = -\mu_v < 0.$$

Since $I_f^* > 0$, $\beta_v > 0$, $\mu_v > 0$, both eigenvalues are negative, indicating stability in the vector dynamics.

Human Block Analysis. The 4×4 human block is complex due to nonlinear terms. Define shorthand notations for clarity:

$$a = \beta_1 \frac{I_f^*\Lambda_v\beta_v}{\mu_v A}, \quad b = \beta_2 I_h^*, \quad c = \beta_3 \frac{F}{\mu_h+\varpi_c}.$$

$$J_{\text{human}} = \begin{pmatrix} -(a+b+c+\mu_h) & 0 & -\beta_2 S_h^* & -\beta_3 S_h^* \\ a & -(\sigma+\delta_1 I_h^*+\mu_h) & -\delta_1 I_f^* & 0 \\ b & -\delta_2 I_f^* & \beta_2 S_h^* - \delta_1 I_h^* - \mu_h - \varpi_h & 0 \\ c & (\delta_1+\delta_2) I_h^* & (\delta_1+\delta_2) I_f^* & \beta_3 S_h^* - \mu_h - \varpi_c \end{pmatrix}. \tag{13}$$

From $f_2 = 0$:

$$\beta_1 S_h^* I_v^* = (\sigma + \delta_1 I_h^* + \mu_h) I_f^* \implies a = I_f^*(\sigma + \delta_1 I_h^* + \mu_h) = -I_f^* J_{22}.$$

From $f_3 = 0$:

$$\beta_2 S_h^* I_h^* = (\delta_2 I_f^* + \mu_h + \varpi_h) I_h^* \implies b = I_h^*(\delta_2 I_f^* + \mu_h + \varpi_h) = I_h^*(-J_{33} + \beta_2 S_h^*).$$

From $f_5 = 0$:

$$\beta_3 S_h^* I_{fh}^* + (\delta_1 + \delta_2) I_f^* I_h^* = (\mu_h + \varpi_c) I_{fh}^*,$$

and since $I_{fh}^* = F/(\mu_h + \varpi_c)$, this is consistent with $F = I_f^* I_h^* (\delta_1 + \delta_2) + E$.

Trace of Human Block:

$$\text{Trace} = J_{11} + J_{22} + J_{33} + J_{44} = -(a+b+c+\mu_h) - (\sigma + \delta_1 I_h^* + \mu_h) + (\beta_2 S_h^* - \delta_2 I_f^* - \mu_h - \varpi_h) + (\beta_3 S_h^* - \mu_h - \varpi_c)$$

$$= -a - b - c - 4\mu_h - \sigma - \delta_1 I_h^* - \delta_2 I_f^* - \varpi_h - \varpi_c + \beta_2 S_h^* + \beta_3 S_h^*.$$

Since $a, b, c, \mu_h, \sigma, \delta_1, \delta_2, \varpi_h, \varpi_c > 0$, and $\beta_2 S_h^*, \beta_3 S_h^* > 0$ but bounded by equilibrium dynamics, the trace is negative if removal rates dominate infection terms. The determinant is intricate and depends on I_f^*, I_h^*, and parameters. For stability, $\det(J_{\text{human}}) > 0$.

Routh-Hurwitz Criteria. For a 4×4 matrix, the characteristic equation is:

$$\lambda^4 + a_1 \lambda^3 + a_2 \lambda^2 + a_3 \lambda + a_4 = 0,$$

where $a_1 = -\text{Trace}$, $a_4 = \det(J_{\text{human}})$. The Routh-Hurwitz criteria for stability are:

- $a_1 > 0$
- $a_3 > 0$
- $a_4 > 0$
- $a_1 a_2 > a_3$
- $(a_1 a_2 - a_3) a_3 > a_1^2 a_4$

Since $a_1 = -\text{Trace} > 0$ (if trace is negative), and $a_4 > 0$ when $R_0 > 1$, we hypothesize stability when $R_0 > 1$, as the endemic equilibrium exists. The endemic equilibrium exists when $R_0 > 1$, indicating sustained disease transmission. Epidemiological models typically show that the endemic equilibrium is stable when $R_0 > 1$, as the disease persists.

3.4. Global Stability Analysis of the Disease-Free Equilibrium. We analyze the global asymptotic stability (GAS) of the disease-free equilibrium (DFE) using the [24] theorem. The theorem states that the DFE is globally asymptotically stable if $R_0 \leq 1$ and:

H1: The system $\dot{W} = F(W,0)$ is globally asymptotically stable at X^*.

H2: The infected dynamics satisfy $G(W,Y) = AY - \hat{G}(W,Y)$, where $A = D_Y G(W^*,0)$ is an M-matrix, and $\hat{G}(W,Y) \geq 0$ in the feasible region Ω.

Partition the system: uninfected $X = (S_h, S_v, R_f, T_{fh})$, infected $Y = (I_f, I_h, I_m, I_{fh}, I_v)$.

$$F(W,Y) = \begin{pmatrix} \Lambda_h - \beta_1 S_h I_v - \beta_2 S_h I_h - \beta_3 S_h I_{fh} - \mu_h S_h \\ \Lambda_v - \beta_v S_v I_f - \mu_v S_v \\ \sigma I_f - \mu_h R_f \\ \varpi_c I_{fh} - \mu_h T_{fh} \end{pmatrix}, \tag{14}$$

$$G(W,Y) = \begin{pmatrix} \beta_1 S_h I_v - \sigma I_f - \delta_1 I_f I_h - \mu_h I_f \\ \beta_2 S_h I_h - \delta_2 I_h I_f - \mu_h I_h - \varpi_h I_h \\ \varpi_h I_h - \mu_h I_m \\ \beta_3 S_h I_{fh} + \delta_1 I_f I_h + \delta_2 I_h I_f - \mu_h I_{fh} - \varpi_c I_{fh} \\ \beta_v S_v I_f - \mu_v I_v \end{pmatrix}. \tag{15}$$

The DFE is $(X^*, 0)$, where $X^* = (\Lambda_h/\mu_h, \Lambda_v/\mu_v, 0, 0)$.

H1: Uninfected System Stability

$$F(W,0) = \begin{pmatrix} \Lambda_h - \mu_h S_h \\ \Lambda_v - \mu_v S_v \\ -\mu_h R_f \\ -\mu_h T_{fh} \end{pmatrix}.$$

Lyapunov function:

$$V_X = \frac{1}{2}\left(S_h - \frac{\Lambda_h}{\mu_h}\right)^2 + \frac{1}{2}\left(S_v - \frac{\Lambda_v}{\mu_v}\right)^2 + \frac{1}{2}R_f^2 + \frac{1}{2}T_{fh}^2,$$

$$\dot{V}_X = \left(S_h - \frac{\Lambda_h}{\mu_h}\right)(\Lambda_h - \mu_h S_h) + \left(S_v - \frac{\Lambda_v}{\mu_v}\right)(\Lambda_v - \mu_v S_v) + R_f(-\mu_h R_f) + T_{fh}(-\mu_h T_{fh})$$

$$= -\mu_h\left(S_h - \frac{\Lambda_h}{\mu_h}\right)^2 - \mu_v\left(S_v - \frac{\Lambda_v}{\mu_v}\right)^2 - \mu_h R_f^2 - \mu_h T_{fh}^2 \leq 0.$$

Equality holds at W^*. By LaSalle's Invariance Principle, H1 is satisfied.

H2: Infected Dynamics

$$A = \begin{pmatrix} -(\sigma+\mu_h) & 0 & 0 & 0 & \beta_1\frac{\Lambda_h}{\mu_h} \\ 0 & \beta_2\frac{\Lambda_h}{\mu_h} - (\mu_h+\varpi_h) & 0 & 0 & 0 \\ 0 & \varpi_h & -\mu_h & 0 & 0 \\ 0 & 0 & 0 & \beta_3\frac{\Lambda_h}{\mu_h} - (\mu_h+\varpi_c) & 0 \\ \beta_v\frac{\Lambda_v}{\mu_v} & 0 & 0 & 0 & -\mu_v \end{pmatrix}, \tag{16}$$

$$\hat{G} = \begin{pmatrix} \beta_1\left(\frac{\Lambda_h}{\mu_h} - S_h\right)I_v + \delta_1 I_f I_h \\ \beta_2\left(\frac{\Lambda_h}{\mu_h} - S_h\right)I_h + \delta_2 I_h I_f \\ 0 \\ \beta_3\left(\frac{\Lambda_h}{\mu_h} - S_h\right)I_{fh} - \delta_1 I_f I_h - \delta_2 I_h I_f \\ \beta_v\left(\frac{\Lambda_v}{\mu_v} - S_v\right)I_f \end{pmatrix}. \tag{17}$$

Since $\hat{G}_4$ may be negative, H2 is not strictly satisfied. Instead, use a Lyapunov function:

$$V_Y = aI_f + bI_h + cI_m + dI_{fh} + eI_v,$$

$$\dot{V}_Y = a[\beta_1 S_h I_v - (\sigma+\mu_h)I_f - \delta_1 I_f I_h] + b[\beta_2 S_h I_h - \delta_2 I_h I_f - (\mu_h+\varpi_h)I_h] + c[\varpi_h I_h - \mu_h I_m]$$

$$+d[\beta_3 S_h I_{fh} + \delta_1 I_f I_h + \delta_2 I_h I_f - (\mu_h+\varpi_c)I_{fh}] + e[\beta_v S_v I_f - \mu_v I_v].$$

Set:

$$e = a\frac{\beta_1\Lambda_h}{\mu_h\mu_v}, \quad c = b\frac{(\mu_h+\varpi_h) - \beta_2\Lambda_h/\mu_h}{\varpi_h}, \quad d = b\frac{(\mu_h+\varpi_h) - \beta_2\Lambda_h/\mu_h}{(\mu_h+\varpi_c) - \beta_3\Lambda_h/\mu_h},$$

assuming:

$$\beta_2\frac{\Lambda_h}{\mu_h} < \mu_h + \varpi_h, \quad \beta_3\frac{\Lambda_h}{\mu_h} < \mu_h + \varpi_c.$$

Then:

$$\dot{V}_Y \leq a(\sigma+\mu_h)\left[\frac{\beta_1\beta_v\Lambda_h\Lambda_v}{(\sigma+\mu_h)\mu_h{\mu_v}^2}-1\right]I_f = a(\sigma+\mu_h)(R_0^2-1)I_f \leq 0 \quad \text{if } R_0 \leq 1.$$

The invariant set where $\dot{V}_Y = 0$ is the DFE, confirming global asymptotic stability when $R_0 \leq 1$.

3.5. Bifurcation Analysis of the Epidemiological Model. We apply the center manifold theorem at $R_0 = 1$ using β_1 as the bifurcation parameter. The system is:

$$\dot{w} = f(w) = \begin{pmatrix} f_1 = \Lambda_h - \beta_1 S_h I_v - \beta_2 S_h I_h - \beta_3 S_h I_{fh} - \mu_h S_h \\ f_2 = \beta_1 S_h I_v - \sigma I_f - \delta_1 I_f I_h - \mu_h I_f \\ f_3 = \beta_2 S_h I_h - \delta_2 I_h I_f - \mu_h I_h - \varpi_h I_h \\ f_4 = \varpi_h I_h - \mu_h I_m \\ f_5 = \beta_3 S_h I_{fh} + \delta_1 I_f I_h + \delta_2 I_h I_f - \mu_h I_{fh} - \varpi_c I_{fh} \\ f_6 = \varpi_c I_{fh} - \mu_h T_{fh} \\ f_7 = \sigma I_f - \mu_h R_f \\ f_8 = \Lambda_v - \beta_v S_v I_f - \mu_v S_v \\ f_9 = \beta_v S_v I_f - \mu_v I_v \end{pmatrix}. \tag{18}$$

The bifurcation parameter is β_{1c}, where:

$$\beta_{1c} = \frac{(\sigma+\mu_h)\mu_v\mu_h\mu_v}{\beta_v\Lambda_h\Lambda_v},$$

ensuring $R_0 = 1$ when $\beta_1 = \beta_{1c}$. At $\beta_1 = \beta_{1c}$, $R_0^2 = 1$. The DFE is $E_0 = (\Lambda_h/\mu_h, 0, 0, 0, 0, 0, 0, \Lambda_v/\mu_v, 0)$.

Theorem 2 [24]: Consider conditions near the DFE at $\beta_1 = \beta_{1c}$:

A1 The Jacobian $A = D_x f(E_0, \beta_{1c})$ has a simple zero eigenvalue, others have negative real parts.

A2 A has nonnegative right eigenvector w and left eigenvector v for the zero eigenvalue.

Bifurcation coefficients:

$$a = \sum_{k,i,j=1}^{9} v_k w_i w_j \frac{\partial^2 f_k}{\partial x_i \partial x_j}(E_0, \beta_{1c}), \quad b = \sum_{k,i=1}^{9} v_k w_i \frac{\partial^2 f_k}{\partial x_i \partial \beta_1}(E_0, \beta_{1c}).$$

The local dynamics depend on a and b:

(i) $a > 0$, $b > 0$: Forward bifurcation.

(iv) $a < 0$, $b > 0$: Backward bifurcation possible.

Proof

Verification of Assumptions A1: The Jacobian at E_0, $\beta_1 = \beta_{1c}$ has a simple zero eigenvalue (confirmed from next-generation matrix and characteristic polynomial analysis). Other eigenvalues are negative under parameter constraints. **A2**: Right and left eigenvectors exist and are nonnegative. Thus, when $R_0 > 1$, a stable endemic equilibrium emerges via forward bifurcation if $a < 0$, $b > 0$. We verify the assumptions of Theorem 2 from [24]:

A1: The Jacobian $A = D_x f(E_0, 0)$ has a simple zero eigenvalue, with all other eigenvalues having negative real parts.

A2: A has right and left eigenvectors w and v for the zero eigenvalue.

A1: Jacobian Analysis. The Jacobian at E_0, $\beta_1 = \beta_{1c}$ is:

(19)

$$A = \begin{pmatrix} -\mu_h & 0 & -\beta_2 \frac{\Lambda_h}{\mu_h} & 0 & -\beta_3 \frac{\Lambda_h}{\mu_h} & 0 & 0 & 0 & -\frac{(\sigma+\mu_h)\mu_v{}^2}{\beta_v \Lambda_v} \\ 0 & -(\sigma+\mu_h) & 0 & 0 & 0 & 0 & 0 & 0 & \frac{(\sigma+\mu_h)\mu_v{}^2}{\beta_v \Lambda_v} \\ 0 & 0 & \beta_2 \frac{\Lambda_h}{\mu_h} - (\mu_h + \varpi_h) & 0 & 0 & 0 & 0 & 0 & 0 \\ 0 & 0 & \varpi_h & -\mu_h & 0 & 0 & 0 & 0 & 0 \\ 0 & 0 & 0 & 0 & \beta_3 \frac{\Lambda_h}{\mu_h} - (\mu_h + \varpi_c) & 0 & 0 & 0 & 0 \\ 0 & 0 & 0 & 0 & \varpi_c & -\mu_h & 0 & 0 & 0 \\ 0 & \sigma & 0 & 0 & 0 & 0 & -\mu_h & 0 & 0 \\ 0 & -\beta_v \frac{\Lambda_v}{\mu_v} & 0 & 0 & 0 & 0 & 0 & -\mu_v & 0 \\ 0 & \beta_v \frac{\Lambda_v}{\mu_v} & 0 & 0 & 0 & 0 & 0 & 0 & -\mu_v \end{pmatrix},$$

where:

$$\beta_1 \frac{\Lambda_h}{\mu_h} = \frac{(\sigma+\mu_h)\mu_v \mu_h \mu_v}{\beta_v \Lambda_h \Lambda_v} \cdot \frac{\Lambda_h}{\mu_h} = \frac{(\sigma+\mu_h)\mu_v{}^2}{\beta_v \Lambda_v}.$$

Compute eigenvalues via $\det(A - \lambda I) = 0$:

- Row 4: $\lambda_4 = -\mu_h$.
- Row 6: $\lambda_6 = -\mu_h$.
- Row 7: $\lambda_7 = -\mu_h$.
- Row 3: $\lambda_3 = \beta_2 \frac{\Lambda_h}{\mu_h} - (\mu_h + \varpi_h) < 0$ if $\beta_2 \Lambda_h < \mu_h(\mu_h + \varpi_h)$.
- Row 5: $\lambda_5 = \beta_3 \frac{\Lambda_h}{\mu_h} - (\mu_h + \varpi_c) < 0$ if $\beta_3 \Lambda_h < \mu_h(\mu_h + \varpi_c)$.
- Row 8: $\lambda_8 = -\mu_v$.

For rows 1, 2, 9:

$$\det\begin{pmatrix} -\mu_h-\lambda & 0 & -\frac{(\sigma+\mu_h)\mu_v{}^2}{\beta_v\Lambda_v} \\ 0 & -(\sigma+\mu_h)-\lambda & \frac{(\sigma+\mu_h)\mu_v{}^2}{\beta_v\Lambda_v} \\ 0 & \beta_v\frac{\Lambda_v}{\mu_v} & -\mu_v-\lambda \end{pmatrix}.$$

Expand along row 1:

$$(-\mu_h-\lambda)\det\begin{pmatrix} -(\sigma+\mu_h)-\lambda & \frac{(\sigma+\mu_h)\mu_v{}^2}{\beta_v\Lambda_v} \\ \beta_v\frac{\Lambda_v}{\mu_v} & -\mu_v-\lambda \end{pmatrix} = (-\mu_h-\lambda)\left[(\sigma+\mu_h+\lambda)(\mu_v+\lambda)-(\sigma+\mu_h)\mu_v\right].$$

At $\lambda = 0$:

$$(\sigma+\mu_h)\mu_v-(\sigma+\mu_h)\mu_v = 0 \implies \lambda_1 = 0.$$

The quadratic factor is:

$$\lambda^2+(\sigma+\mu_h+\mu_v)\lambda+(\sigma+\mu_h)\mu_v = 0,$$

with positive coefficients, so roots have negative real parts. Row 1 also gives $\lambda_9 = -\mu_h$. Thus, eigenvalues are:

$$\lambda_1 = 0, \quad \lambda_3 = \beta_2\frac{\Lambda_h}{\mu_h}-(\mu_h+\varpi_h), \quad \lambda_4 = \lambda_6 = \lambda_7 = \lambda_9 = -\mu_h,$$

$$\lambda_5 = \beta_3\frac{\Lambda_h}{\mu_h}-(\mu_h+\varpi_c), \quad \lambda_8 = -\mu_v,$$

and two other negative roots. Assuming:

$$\beta_2\frac{\Lambda_h}{\mu_h} < \mu_h+\varpi_h, \quad \beta_3\frac{\Lambda_h}{\mu_h} < \mu_h+\varpi_c,$$

all non-zero eigenvalues are negative, satisfying A1.

A2: Eigenvectors.

Right eigenvector w, $Aw = 0$:

$$w^T = \left(-\frac{(\sigma+\mu_h)\mu_v{}^2}{\mu_h\beta_v\Lambda_v},0,0,0,0,0,0,0,1\right). \tag{20}$$

Left eigenvector v, $vA = 0$:

$$v^T = (0,\mu_v,0,0,0,0,0,0,\beta_v\Lambda_v). \tag{21}$$

Both are nonnegative. A2 is satisfied.

Direct Calculation of Bifurcation Coefficients.

$$a = \sum_{k,i,j=1}^{9} v_k w_i w_j \frac{\partial^2 f_k}{\partial x_i \partial x_j}(E_0,0), \quad b = \sum_{k,i=1}^{9} v_k w_i \frac{\partial^2 f_k}{\partial x_i \partial \beta_1}(E_0,0). \tag{22}$$

Non-zero second derivatives at E_0:

- f_1: $\frac{\partial^2 f_1}{\partial S_h \partial I_v} = -\beta_{1c}$, $\frac{\partial^2 f_1}{\partial S_h \partial I_h} = -\beta_2$, $\frac{\partial^2 f_1}{\partial S_h \partial I_{fh}} = -\beta_3$,
- f_2: $\frac{\partial^2 f_2}{\partial S_h \partial I_v} = \beta_{1c}$, $\frac{\partial^2 f_2}{\partial I_f \partial I_h} = -\delta_1$,
- f_3: $\frac{\partial^2 f_3}{\partial S_h \partial I_h} = \beta_2$, $\frac{\partial^2 f_3}{\partial I_h \partial I_f} = -\delta_2$,
- f_5: $\frac{\partial^2 f_5}{\partial S_h \partial I_{fh}} = \beta_3$, $\frac{\partial^2 f_5}{\partial I_f \partial I_h} = \delta_1 + \delta_2$,
- f_8: $\frac{\partial^2 f_8}{\partial S_v \partial I_f} = -\beta_v$,
- f_9: $\frac{\partial^2 f_9}{\partial S_v \partial I_f} = \beta_v$.

$$a = v_2 \left(w_1 w_9 \frac{\partial^2 f_2}{\partial S_h \partial I_v} \right) + v_9 \left(w_8 w_9 \frac{\partial^2 f_9}{\partial S_v \partial I_f} \right).$$

Since $w_3 = w_8 = 0$:

$$a = v_2 w_1 w_9 \beta_{1c} = \mu_v \left(-\frac{(\sigma+\mu_h){\mu_v}^2}{\mu_h \beta_v \Lambda_v} \right)(1)\beta_{1c} = -\frac{(\sigma+\mu_h){\mu_v}^3 \beta_{1c}}{\mu_h \beta_v \Lambda_v} < 0. \tag{23}$$

For b:

$$\frac{\partial^2 f_2}{\partial S_h \partial \beta_1} = I_v = 0 \text{ at } E_0 \implies b = v_2 w_1 \cdot 0 = 0.$$

Since $b = 0$, direct calculation is inconclusive. We proceed with center manifold analysis.

Center Manifold Analysis. Focus on infected variables I_f, I_v:

$$\dot{I}_f = \beta_{1c} S_h I_v - (\sigma+\mu_h) I_f, \quad \dot{I}_v = \beta_v S_v I_f - \mu_v I_v.$$

Near E_0, let:

$$I_f = c w_2 = c\mu_v, \quad I_v = c w_9 = c\beta_v \Lambda_v,$$

$$S_h = \frac{\Lambda_h}{\mu_h} + h(c), \quad S_v = \frac{\Lambda_v}{\mu_v} + g(c).$$

From $f_1 = 0$:

$$\Lambda_h - \beta_{1c}\left(\frac{\Lambda_h}{\mu_h} + h\right)(c\beta_v \Lambda_v) - \mu_h \left(\frac{\Lambda_h}{\mu_h} + h\right) = 0,$$

$$h \approx -\frac{(\sigma+\mu_h){\mu_v}^3 c}{\mu_h \beta_v \Lambda_v}.$$

From $f_8 = 0$:

$$g \approx -\frac{\beta_v \Lambda_v c}{\mu_v}.$$

Substitute into $\dot{I}_f$:

$$\dot{I}_f = \beta_{1c}\left(\frac{\Lambda_h}{\mu_h} - \frac{(\sigma+\mu_h){\mu_v}^3 c}{\mu_h \beta_v \Lambda_v}\right)(\beta_v \Lambda_v c) - (\sigma+\mu_h)(c\mu_v) = (\sigma+\mu_h)\mu_v c - \frac{(\sigma+\mu_h)^2 {\mu_v}^3 \beta_v \Lambda_v}{\mu_h} c^2 + O(c^3).$$

Project onto center manifold:

$$\dot{c} = \frac{(\sigma+\mu_h){\mu_v}^2}{\beta_v \Lambda_v} c - \frac{(\sigma+\mu_h)^2 {\mu_v}^3 \beta_v \Lambda_v}{\mu_h} c^2 + O(c^3).$$

Comparing with $\dot{c} = bc + \frac{a}{2}c^2$:

$$b = \frac{(\sigma+\mu_h){\mu_v}^2}{\beta_v \Lambda_v} > 0, \quad a = -2\frac{(\sigma+\mu_h)^2 {\mu_v}^3 \beta_v \Lambda_v}{\mu_h} < 0. \tag{24}$$

With $a < 0$, $b > 0$, case (iv) of Theorem 2 from [24]applies: the DFE is stable for $R_0 < 1$, unstable for $R_0 > 1$, and a positive, stable endemic equilibrium emerges for $R_0 > 1$. This confirms a forward transcritical bifurcation.

3.6. Fractional Stochastic Model. In this section, a fractional stochastic model in the form of the Atangana–Baleanu–Caputo (ABC) operator is incorporated to explore the randomness dynamics in the HIV/AIDS and filariasis co-infection model:

$$\begin{aligned}
{}_0^{ABC}D^{\tau} S_h &= \left(\Lambda_h^{\tau} - \beta_1^{\tau} S_h I_v - \beta_2^{\tau} S_h I_h - \beta_3^{\tau} S_h I_{fh} - \mu_h^{\tau} S_h\right) dt + A_1 P_1(t, S_h)\, dQ_1(t),\\
{}_0^{ABC}D^{\tau} I_f &= \left(\beta_1^{\tau} S_h I_v - \delta_2^{\tau} I_f I_h - (\sigma^{\tau} + \mu_h^{\tau}) I_f\right) dt + A_2 P_2(t, I_f)\, dQ_2(t),\\
{}_0^{ABC}D^{\tau} I_h &= \left(\beta_2^{\tau} S_h I_h - \delta_1^{\tau} I_f I_h - (\varpi_h^{\tau} + \mu_h^{\tau}) I_h\right) dt + A_3 P_3(t, I_h)\, dQ_3(t),\\
{}_0^{ABC}D^{\tau} I_m &= \left(\varpi_h^{\tau} I_h - \mu_h^{\tau} I_m\right) dt + A_4 P_4(t, I_m)\, dQ_4(t),\\
{}_0^{ABC}D^{\tau} I_{fh} &= \left(\beta_3^{\tau} S_h I_{fh} + \delta_1^{\tau} I_f I_h + \delta_2^{\tau} I_h I_f - (\varpi_c^{\tau} + \mu_h^{\tau}) I_{fh}\right) dt + A_5 P_5(t, I_{fh})\, dQ_5(t),\\
{}_0^{ABC}D^{\tau} T_{fh} &= \left(\varpi_c^{\tau} I_{fh} - \mu_h^{\tau} T_{fh}\right) dt + A_6 P_6(t, T_{fh})\, dQ_6(t),\\
{}_0^{ABC}D^{\tau} R_f &= \left(\sigma^{\tau} I_f - \mu_h^{\tau} R_f\right) dt + A_7 P_7(t, R_f)\, dQ_7(t),\\
{}_0^{ABC}D^{\tau} S_v &= \left(\Lambda_v^{\tau} - \beta_v^{\tau} S_v I_f - \mu_v^{\tau} S_v\right) dt + A_8 P_8(t, S_v)\, dQ_8(t),\\
{}_0^{ABC}D^{\tau} I_v &= \left(\beta_v^{\tau} S_v I_f - \mu_v^{\tau} I_v\right) dt + A_9 P_9(t, I_v)\, dQ_9(t).
\end{aligned} \tag{25}$$

where $Q_1(t), Q_2(t), \ldots, Q_9(t)$ represent independent standard Brownian motions, and $A_1, A_2, \ldots, A_9$ are stochastic intensity constants.

3.7. Existence and Uniqueness of Solution. To establish the existence and uniqueness of the solution to the co-infected model, we reformulate the system as:

$$
\begin{aligned}
{}_0^{ABC}D^{\tau}S_h &= K_1(t,S_h)\,dt + A_1P_1(t,S_h)\,dQ_1(t),\\
{}_0^{ABC}D^{\tau}I_f &= K_2(t,I_f)\,dt + A_2P_2(t,I_f)\,dQ_2(t),\\
{}_0^{ABC}D^{\tau}I_h &= K_3(t,I_h)\,dt + A_3P_3(t,I_h)\,dQ_3(t),\\
{}_0^{ABC}D^{\tau}I_m &= K_4(t,I_m)\,dt + A_4P_4(t,I_m)\,dQ_4(t),\\
{}_0^{ABC}D^{\tau}I_{fh} &= K_5(t,I_{fh})\,dt + A_5P_5(t,I_{fh})\,dQ_5(t),\\
{}_0^{ABC}D^{\tau}T_{fh} &= K_6(t,T_{fh})\,dt + A_6P_6(t,T_{fh})\,dQ_6(t),\\
{}_0^{ABC}D^{\tau}R_f &= K_7(t,R_f)\,dt + A_7P_7(t,R_f)\,dQ_7(t),\\
{}_0^{ABC}D^{\tau}S_v &= K_8(t,S_v)\,dt + A_8P_8(t,S_v)\,dQ_8(t),\\
{}_0^{ABC}D^{\tau}I_v &= K_9(t,I_v)\,dt + A_9P_9(t,I_v)\,dQ_9(t).
\end{aligned}
\tag{26}
$$

We show that for $i \in \{1,2,\ldots,9\}$,

$$
|K_i(t,z_i)|^2 \le H_i(1+|z_i|^2), \quad |A_i(t,z_i)|^2 \le H_i(1+|z_i|^2), \quad \forall t \in [0,T],
$$

and

$$
|K_i(t,z_i^1) - K_i(t,z_i^2)|^2 \le \bar{H}_i|z_i^1 - z_i^2|^2, \quad |A_i(t,z_i^1) - A_i(t,z_i^2)|^2 \le \bar{H}_i|z_i^1 - z_i^2|^2, \quad \forall t \in [0,T].
$$

In this regard, the Lipschitz condition is examined as follows:

$$
\begin{aligned}
\left|K_1(t,S_h)\right|^2 &= \left|\Lambda_h^{\tau} - \beta_1^{\tau}S_hI_v - \beta_2^{\tau}S_hI_h - \beta_3^{\tau}S_hI_{fh} - \mu_h^{\tau}S_h\right|^2\\
&\le 3\left(\Lambda_h^{\tau 2} + 3(\beta_1^{\tau 2}|S_h|^2|I_v|^2 + \beta_2^{\tau 2}|S_h|^2|I_h|^2 + \beta_3^{\tau 2}|S_h|^2\left|I_{fh}\right|^2) + \mu_h^{\tau 2}|S_h|^2\right)\\
&\le 3\left(\Lambda_h^{\tau 2} + 3\left(\beta_1^{\tau 2}(\sup_{0<t<T}|I_v|^2) + \beta_2^{\tau 2}(\sup_{0<t<T}|I_h|^2) + \beta_3^{\tau 2}(\sup_{0<t<T}\left|I_{fh}\right|^2) + \mu_h^{\tau 2}\right)|S_h|^2\right)\\
&\le 3\left(\Lambda_h^{\tau 2} + 3(\beta_1^{\tau 2}\left\|I_v^2\right\|\infty + \beta_2^{\tau 2}\left\|I_h^2\right\|\infty + \beta_3^{\tau 2}\left\|I_{fh}^2\right\|_{\infty} + \mu_h^{\tau 2})|S_h|^2\right)
\end{aligned}
$$

$$\leq 3\Lambda_h^{\tau 2}\left(1+3\frac{\beta_1^{\tau 2}\left\|I_v^2\right\|\infty+\beta_2^{\tau 2}\left\|I_h^2\right\|\infty+\beta_3^{\tau 2}\left\|I_{fh}^2\right\|_\infty+\mu_h^{\tau 2}}{\Lambda_h^{\tau 2}}|S_h|^2\right). \tag{27}$$

Under the condition that

$$\frac{\beta_1^{\tau 2}\left\|I_v^2\right\|\infty+\beta_2^{\tau 2}\left\|I_h^2\right\|\infty+\beta_3^{\tau 2}\left\|I_{fh}^2\right\|_\infty+\mu_h^{\tau 2}}{\Lambda_h^{\tau 2}}<1,$$

it can be written as

$$\left|K_1(t,S_h)\right|^2\leq H_1(1+|S_h|^2).$$

$$\begin{aligned}
\left|K_2(t,I_f)\right|^2&=\left|\beta_1^\tau S_hI_v-\delta_2^\tau I_fI_h-(\sigma^\tau+\mu_h^\tau)I_f\right|^2\\
&\leq 3(\beta_1^{\tau 2}|S_h|^2|I_v|^2+\delta_2^{\tau 2}\left|I_f\right|^2|I_h|^2+(\sigma^\tau+\mu_h^\tau)^2\left|I_f\right|^2)\\
&\leq 3\left(\beta_1^{\tau 2}(\sup_{0<t<T}|S_h|^2)(\sup_{0<t<T}|I_v|^2)+\delta_2^{\tau 2}(\sup_{0<t<T}|I_h|^2)+(\sigma^\tau+\mu_h^\tau)^2\right)\left|I_f\right|^2\\
&\leq 3\left(\beta_1^{\tau 2}\left\|S_h^2\right\|\infty\left\|I_v^2\right\|\infty+\delta_2^{\tau 2}\left\|I_h^2\right\|_\infty+(\sigma^\tau+\mu_h^\tau)^2\right)\left|I_f\right|^2\\
&\leq 3\beta_1^{\tau 2}\left\|S_h^2\right\|\infty\left\|I_v^2\right\|\infty\left(1+\frac{\delta_2^{\tau 2}\left\|I_h^2\right\|\infty+(\sigma^\tau+\mu_h^\tau)^2}{\beta_1^{\tau 2}\left\|S_h^2\right\|\infty\left\|I_v^2\right\|_\infty}\left|I_f\right|^2\right).
\end{aligned}\tag{28}$$

Under the condition that

$$\frac{\delta_2^{\tau 2}\left\|I_h^2\right\|\infty+(\sigma^\tau+\mu_h^\tau)^2}{\beta_1^{\tau 2}\left\|S_h^2\right\|\infty\left\|I_v^2\right\|_\infty}\left|I_f\right|^2<1,$$

it can be written as

$$\left|K_2(t,I_f)\right|^2\leq H_2^\tau(1+\left|I_f\right|^2).$$

$$\begin{aligned}
\left|K_3(t,I_h)\right|^2&=\left|\beta_2^\tau S_hI_h-\delta_1^\tau I_fI_h-(\varpi_h^\tau+\mu_h^\tau)I_h\right|^2\\
&\leq 3(\beta_2^{\tau 2}|S_h|^2|I_h|^2+\delta_1^{\tau 2}\left|I_f\right|^2|I_h|^2+(\varpi_h^\tau+\mu_h^\tau)^2|I_h|^2)\\
&\leq 3\left(\beta_2^{\tau 2}(\sup_{0<t<T}|S_h|^2)+\delta_1^{\tau 2}(\sup_{0<t<T}\left|I_f\right|^2)+(\varpi_h^\tau+\mu_h^\tau)^2\right)|I_h|^2\\
&\leq 3\left(\beta_2^{\tau 2}\left\|S_h^2\right\|\infty+\delta_1^{\tau 2}\left\|I_f^2\right\|\infty+(\varpi_h^\tau+\mu_h^\tau)^2\right)|I_h|^2\\
&\leq 3\beta_2^{\tau 2}\left\|S_h^2\right\|\infty\left(1+\frac{\delta_1^{\tau 2}\left\|I_f^2\right\|\infty+(\varpi_h^\tau+\mu_h^\tau)^2}{\beta_2^{\tau 2}\left\|S_h^2\right\|_\infty}|I_h|^2\right).
\end{aligned}\tag{29}$$

Under the condition that

$$\frac{\delta_1^{\tau 2}\left\|I_f^2\right\|\infty+(\varpi_h^\tau+\mu_h^\tau)^2}{\beta_2^{\tau 2}\left\|S_h^2\right\|\infty}|I_h|^2<1,$$

it can be written as

$$\left|K_3(t,I_h)\right|^2\le H_3^\tau(1+|I_h|^2).$$

$$\begin{aligned}\left|K_4(t,I_m)\right|^2&=\left|\varpi_h^\tau I_h-\mu_h^\tau I_m\right|^2\\&\le 2(\varpi_h^{\tau 2}|I_h|^2+\mu_h^{\tau 2}|I_m|^2)\\&\le 2\left(\varpi_h^{\tau 2}(\sup_{0<t<T}|I_h|^2)+\mu_h^{\tau 2}\right)|I_m|^2\\&\le 2(\varpi_h^{\tau 2}\left\|I_h^2\right\|_\infty+\mu_h^{\tau 2}|I_m|^2)\\&\le 2\varpi_h^{\tau 2}\left\|I_h^2\right\|\infty\left(1+\frac{\mu_h^{\tau 2}}{\varpi_h^{\tau 2}\left\|I_h^2\right\|\infty}|I_m|^2\right).\end{aligned}\tag{30}$$

Under the condition that

$$\frac{\mu_h^{\tau 2}}{\varpi_h^{\tau 2}\left\|I_h^2\right\|_\infty}|I_m|^2<1,$$

it can be written as

$$\left|K_4(t,I_m)\right|^2\le H_4(1+|I_m|^2).$$

$$\begin{aligned}\left|K_5(t,I_{fh})\right|^2&=\left|\beta_3^\tau S_hI_{fh}-\delta_2^\tau I_fI_h-\delta_1^\tau I_fI_h-(\varpi_c^\tau+\mu_h^\tau)I_{fh}\right|^2\\&\le 3\left(\beta_3^{\tau 2}|S_h|^2\left|I_{fh}\right|^2+2(\delta_1^{\tau 2}\left|I_f\right|^2|I_h|^2+\delta_2^{\tau 2}\left|I_f\right|^2\left|I_{fh}\right|^2)+(\varpi_c^\tau+\mu_h^\tau)^2\left|I_{fh}\right|^2\right)\\&\le 3\Bigg(\beta_3^{\tau 2}(\sup_{0<t<T}|S_h|^2)\left|I_{fh}\right|^2+2\delta_1^{\tau 2}(\sup_{0<t<T}\left|I_f\right|^2)(\sup_{0<t<T}|I_h|^2)+2\delta_2^{\tau 2}(\sup_{0<t<T}\left|I_f\right|^2)(\sup_{0<t<T}\left|I_{fh}\right|^2)\\&\quad+(\varpi_c^\tau+\mu_h^\tau)^2\left|I_{fh}\right|^2\Bigg)\\&\le 3\left(\beta_3^{\tau 2}\left\|S_h^2\right\|\infty+2(\delta_1^{\tau 2}\left\|I_f^2\right\|\infty\left\|I_h^2\right\|\infty+\delta_2^{\tau 2}\left\|I_f^2\right\|\infty\left\|I_{fh}^2\right\|\infty)+(\varpi_c^\tau+\mu_h^\tau)^2\right)\left|I_{fh}\right|^2\\&\le 3\cdot 2(\delta_1^{\tau 2}\left\|S_h^2\right\|\infty\left\|I_h^2\right\|\infty+\delta_2^{\tau 2}\left\|I_f^2\right\|\infty\left\|I_h^2\right\|\infty)\left(1+\frac{\beta_3^{\tau 2}\left\|S_h^2\right\|\infty+(\varpi_c^\tau+\mu_h^\tau)^2}{2(\delta_1^{\tau 2}\|S_h^2\|_\infty\|I_h^2\|_\infty+\delta_2^{\tau 2}\left\|I_f^2\right\|_\infty\|I_h^2\|_\infty)}\left|I_{fh}\right|^2\right).\end{aligned}\tag{31}$$

Under the condition that

$$\frac{\beta_3^{\tau 2}\left\|S_h^2\right\|\infty+(\varpi_c^\tau+\mu_h^\tau)^2}{2(\delta_1^{\tau 2}\left\|S_h^2\right\|\infty\left\|I_h^2\right\|\infty+\delta_2^{\tau 2}\left\|I_f^2\right\|\infty\left\|I_h^2\right\|\infty)}\left|I_{fh}\right|^2<1,$$

it can be written as

$$\left|K_5(t,I_{fh})\right|^2 \leq H_5^{\tau}(1+\left|I_{fh}\right|^2).$$

$$\begin{aligned}
\left|K_6(t,T_{fh})\right|^2 &= \left|\varpi_c^{\tau} I_{fh} - \mu_h^{\tau} T_{fh}\right|^2 \\
&\leq 2(\varpi_c^{\tau 2}\left|I_{fh}\right|^2 + \mu_h^{\tau 2}\left|T_{fh}\right|^2) \\
&\leq 2\left(\varpi_c^{\tau 2}(\sup_{0<t<T}\left|I_{fh}\right|^2) + \mu_h^{\tau 2}\right)\left|T_{fh}\right|^2 \\
&\leq 2(\varpi_c^{\tau 2}\left\|I_{fh}^2\right\|\infty + \mu_h^{\tau 2}\left|T_{fh}\right|^2) \\
&\leq 2\varpi_c^{\tau 2}\left\|I_{fh}^2\right\|\infty\left(1+\frac{\mu_h^{\tau 2}}{\varpi_c^{\tau 2}\left\|I_{fh}^2\right\|\infty}\left|T_{fh}\right|^2\right). \qquad (32)
\end{aligned}$$

Under the condition that

$$\frac{\mu_h^{\tau 2}}{\varpi_c^{\tau 2}\left\|I_{fh}^2\right\|\infty}\left|T_{fh}\right|^2 < 1,$$

it can be written as

$$\left|K_6(t,T_{fh})\right|^2 \leq H_6^{\tau}(1+\left|T_{fh}\right|^2).$$

$$\begin{aligned}
\left|K_7(t,R_f)\right|^2 &= \left|\sigma^{\tau} I_f - \mu_h^{\tau} R_f\right|^2 \\
&\leq 2(\sigma^{\tau 2}\left|I_f\right|^2 + \mu_h^{\tau 2}\left|R_f\right|^2) \\
&\leq 2\left(\sigma^{\tau 2}(\sup_{0<t<T}\left|I_f\right|^2) + \mu_h^{\tau 2}\right)\left|R_f\right|^2 \\
&\leq 2(\sigma^{\tau 2}\left\|I_f^2\right\|_{\infty} + \mu_h^{\tau 2}\left|R_f\right|^2) \\
&\leq 2\sigma^{\tau 2}\left\|I_f^2\right\|_{\infty}\left(1+\frac{\mu_h^{\tau 2}}{\sigma^{\tau 2}\left\|I_f^2\right\|_{\infty}}\left|R_f\right|^2\right). \qquad (33)
\end{aligned}$$

Under the condition that

$$\frac{\mu_h^{\tau 2}}{\sigma^{\tau 2}\left\|I_f^2\right\|_{\infty}}\left|R_f\right|^2 < 1,$$

it can be written as

$$\left|K_7(t,R_f)\right|^2 \leq H_7(1+\left|R_f\right|^2).$$

$$
\begin{aligned}
\left|K_8(t,S_v)\right|^2 &= \left|\Lambda_v^\tau - \beta_v^\tau S_v I_f - \mu_v^\tau S_v\right|^2 \\
&\leq 3(\Lambda_v^{\tau 2} + \beta_v^{\tau 2}|S_v|^2\left|I_f\right|^2 + \mu_v^{\tau 2}|S_v|^2) \\
&\leq 3\left(\Lambda_v^{\tau 2} + \beta_v^{\tau 2}(\sup_{0<t<T}\left|I_f\right|^2)|S_v|^2 + \mu_v^{\tau 2}|S_v|^2\right) \\
&\leq 3\left(\Lambda_v^{\tau 2} + (\beta_v^{\tau 2}\left\|I_f^2\right\|_\infty + \mu_v^{\tau 2})|S_v|^2\right) \\
&\leq 3\Lambda_v^{\tau 2}\left(1 + \frac{\beta_v^{\tau 2}\left\|I_f^2\right\|_\infty + \mu_v^{\tau 2}}{\Lambda_v^{\tau 2}}|S_v|^2\right). \qquad (34)
\end{aligned}
$$

Under the condition that

$$
\frac{\beta_v^{\tau 2}\left\|I_f^2\right\|_\infty + \mu_v^{\tau 2}}{\Lambda_v^{\tau 2}}|S_v|^2 < 1,
$$

it can be written as

$$
\left|K_8(t,S_v)\right|^2 \leq H_8(1+|S_v|^2).
$$

$$
\begin{aligned}
\left|K_9(t,I_v)\right|^2 &= \left|\beta_v^\tau S_v I_f - \mu_v^\tau I_v\right|^2 \\
&\leq 2(\beta_v^{\tau 2}|S_v|^2\left|I_f\right|^2 + \mu_v^{\tau 2}|I_v|^2) \\
&\leq 2\left(\beta_v^{\tau 2}(\sup_{0<t<T}|S_v|^2)(\sup_{0<t<T}\left|I_f\right|^2) + \mu_v^{\tau 2}\right)|I_v|^2 \\
&\leq 2(\beta_v^{\tau 2}\left\|S_v^2\right\|_\infty\left\|I_f^2\right\|_\infty + \mu_v^{\tau 2}|I_v|^2) \\
&\leq 2\beta_v^{\tau 2}\left\|S_v^2\right\|_\infty\left\|I_f^2\right\|_\infty\left(1 + \frac{\mu_v^{\tau 2}}{\beta_v^{\tau 2}\left\|S_v^2\right\|_\infty\left\|I_f^2\right\|_\infty}|I_v|^2\right). \qquad (35)
\end{aligned}
$$

Under the condition that

$$
\frac{\mu_v^{\tau 2}}{\beta_v^{\tau 2}\left\|S_v^2\right\|_\infty\left\|I_f^2\right\|_\infty}|I_v|^2 < 1,
$$

it can be written as

$$
\left|K_9(t,I_v)\right|^2 \leq H_9(1+|I_v|^2).
$$

Following $\forall t \in [0,T]$, we obtain:

$$
\left|A_1(t,S_h)\right|^2 = {p_1}^2|S_h|^2 \leq \rho_1^{\tau 2}(1+|S_h|^2),
$$

$$
\left|A_2(t,I_f)\right|^2 \leq {p_2}^2(1+\left|I_f\right|^2),
$$

$$\begin{aligned}
\left|A_3(t,I_h)\right|^2 &\leq p_3^2(1+|I_h|^2),\\
\left|A_4(t,I_m)\right|^2 &\leq {p_4}^2(1+|I_m|^2),\\
\left|A_5(t,I_{fh})\right|^2 &\leq {p_5}^2(1+\left|I_{fh}\right|^2),\\
\left|A_6(t,T_{fh})\right|^2 &\leq p_6^2(1+\left|T_{fh}\right|^2),\\
\left|A_7(t,R_f)\right|^2 &\leq p_7^2(1+\left|R_f\right|^2),\\
\left|A_8(t,S_v)\right|^2 &\leq {p_8}^2|S_v|^2 \leq \rho_8^{\tau 2}(1+|S_v|^2),\\
\left|A_9(t,I_v)\right|^2 &\leq {p_9}^2(1+|I_v|^2).
\end{aligned}$$

Under the Lipschitz condition, the following condition is confirmed, for which:

$$(K_i(t,z_i))i \in \{1,\ldots,9\}, \quad (A_i^{\tau}(t,z_i))i \in \{1,\ldots,9\}.$$

$$\begin{aligned}
&\left|K_1(t,S_{h1})-K_1(t,S_{h2})\right|^2\\
&=\left|(-\beta_1^{\tau}I_v-\beta_2^{\tau}I_h-\beta_3^{\tau}I_{fh}-\mu_h^{\tau})(S_{h1}-S_{h2})\right|^2\\
&\leq 2\left(3(\beta_1^{\tau 2}|I_v|^2+\beta_2^{\tau 2}|I_h|^2+\beta_3^{\tau 2}\left|I_{fh}\right|^2)+\mu_h^{\tau 2}\right)|S_{h1}-S_{h2}|^2\\
&\leq 2\left(3(\beta_1^{\tau 2}(\sup_{0<t<T}|I_v|^2)+\beta_2^{\tau 2}(\sup_{0<t<T}|I_h|^2)+\beta_3^{\tau 2}(\sup_{0<t<T}\left|I_{fh}\right|^2))+\mu_h^{\tau 2}\right)|S_{h1}-S_{h2}|^2\\
&\leq 2\left(3(\beta_1^{\tau 2}\left\|I_v^2\right\|_{\infty}+\beta_2^{\tau 2}\left\|I_h^2\right\|_{\infty}+\beta_3^{\tau 2}\left\|I_{fh}^2\right\|_{\infty})+\mu_h^{\tau 2}\right)|S_{h1}-S_{h2}|^2\\
&\leq \overline{K}_1|S_{h1}-S_{h2}|^2. \qquad (36)
\end{aligned}$$

$$\begin{aligned}
\left|K_2(t,I_{f1})-K_2(t,I_{f2})\right|^2 &=\left|(-\delta_2^{\tau}I_h-(\sigma^{\tau}+\mu_h^{\tau}))(I_{f1}-I_{f2})\right|^2\\
&\leq 2(\delta_2^{\tau 2}|I_h|^2+(\sigma^{\tau}+\mu_h^{\tau})^2)\left|I_{f1}-I_{f2}\right|^2\\
&\leq 2\left(\delta_2^{\tau 2}(\sup_{0<t<T}|I_h|^2)+(\sigma^{\tau}+\mu_h^{\tau})^2\right)\left|I_{f1}-I_{f2}\right|^2\\
&\leq 2(\delta_2^{\tau 2}\left\|I_h^2\right\|_{\infty}+(\sigma^{\tau}+\mu_h^{\tau})^2)\left|I_{f1}-I_{f2}\right|^2\\
&\leq \overline{K}_2\left|I_{f1}-I_{f2}\right|^2. \qquad (37)
\end{aligned}$$

$$\begin{aligned}\left|K_3(t,I_{h1})-K_3(t,I_{h2})\right|^2 &= \left|(\beta_2^\tau S_h-\delta_1^\tau I_f-(\varpi_h^\tau+\mu_h^\tau))(I_{h1}-I_{h2})\right|^2\\ &\le 3(\beta_2^{\tau 2}|S_h|^2+\delta_1^{\tau 2}\left|I_f\right|^2+(\varpi_h^\tau+\mu_h^\tau)^2)|I_{h1}-I_{h2}|^2\\ &\le 3\left(\beta_2^{\tau 2}(\sup_{0<t<T}|S_h|^2)+\delta_1^{\tau 2}(\sup_{0<t<T}\left|I_f\right|^2)+(\varpi_h^\tau+\mu_h^\tau)^2\right)|I_{h1}-I_{h2}|^2\\ &\le 3(\beta_2^{\tau 2}\left\|S_h^2\right\|_\infty+\delta_1^{\tau 2}\left\|I_f^2\right\|_\infty+(\varpi_h^\tau+\mu_h^\tau)^2)|I_{h1}-I_{h2}|^2\\ &\le \overline{K}_3|I_{h1}-I_{h2}|^2. \end{aligned} \tag{38}$$

$$\begin{aligned}\left|K_4(t,I_{m1})-K_4(t,I_{m2})\right|^2 &= \left|-\mu_h^\tau(I_{m1}-I_{m2})\right|^2\\ &\le \mu_h^{\tau 2}|I_{m1}-I_{m2}|^2\\ &\le \overline{K}_4|I_{m1}-I_{m2}|^2. \end{aligned} \tag{39}$$

$$\begin{aligned}\left|K_5(t,I_{fh1})-K_5(t,I_{fh2})\right|^2 &= \left|(\beta_3^\tau S_h-(\varpi_c^\tau+\mu_h^\tau))(I_{fh1}-I_{fh2})\right|^2\\ &\le 2(\beta_3^{\tau 2}|S_h|^2+(\varpi_c^\tau+\mu_h^\tau)^2)\left|I_{fh1}-I_{fh2}\right|^2\\ &\le 2\left(\beta_3^{\tau 2}(\sup_{0<t<T}|S_h|^2)+(\varpi_c^\tau+\mu_h^\tau)^2\right)\left|I_{fh1}-I_{fh2}\right|^2\\ &\le 2(\beta_3^{\tau 2}\left\|S_h^2\right\|_\infty+(\varpi_c^\tau+\mu_h^\tau)^2)\left|I_{fh1}-I_{fh2}\right|^2\\ &\le \overline{K}_5\left|I_{fh1}-I_{fh2}\right|^2. \end{aligned} \tag{40}$$

$$\begin{aligned}\left|K_6(t,T_{fh1})-K_6(t,T_{fh2})\right|^2 &= \left|-\mu_h^\tau(T_{fh1}-T_{fh2})\right|^2\\ &\le \mu_h^{\tau 2}\left|T_{fh1}-T_{fh2}\right|^2\\ &\le \overline{K}_6\left|T_{fh1}-T_{fh2}\right|^2. \end{aligned} \tag{41}$$

$$\begin{aligned}\left|K_7(t,R_{f1})-K_7(t,R_{f2})\right|^2 &= \left|-\mu_h^\tau(R_{f1}-R_{f2})\right|^2\\ &\le \mu_h^{\tau 2}\left|R_{f1}-R_{f2}\right|^2\\ &\le \overline{K}_7\left|R_{f1}-R_{f2}\right|^2. \end{aligned} \tag{42}$$

$$\begin{aligned}\left|K_8(t,S_{v1})-K_8(t,S_{v2})\right|^2 &= \left|(-\beta_v^{\tau}I_f-\mu_v^{\tau})(S_{v1}-S_{v2})\right|^2\\ &\le 2(\beta_v^{\tau 2}\left|I_f\right|^2+\mu_v^{\tau 2})|S_{v1}-S_{v2}|^2\\ &\le 2\left(\beta_v^{\tau 2}(\sup_{0<t<T}\left|I_f\right|^2)+\mu_v^{\tau 2}\right)|S_{v1}-S_{v2}|^2\\ &\le 2(\beta_v^{\tau 2}\left\|I_f^2\right\|\infty+\mu_v^{\tau 2})|S_{v1}-S_{v2}|^2\\ &\le \overline{K}_8|S_{v1}-S_{v2}|^2. \end{aligned} \tag{43}$$

$$\begin{aligned}\left|K_9(t,I_{v1})-K_9(t,I_{v2})\right|^2 &= \left|-\mu_v^{\tau}(I_{v1}-I_{v2})\right|^2\\ &\le \mu_v^{\tau 2}|I_{v1}-I_{v2}|^2\\ &\le \overline{K}_9|I_{v1}-I_{v2}|^2. \end{aligned} \tag{44}$$

$$\begin{aligned}\left|A_1(t,S_{h1})-A_1(t,S_{h2})\right| &\le \frac{3}{2}p_1^2|S_{h1}-S_{h2}|^2 \le \overline{H}_1|S_{h1}-S_{h2}|^2,\\ \left|A_2(t,I_{f1})-A_2(t,I_{f2})\right| &\le \frac{3}{2}p_2^2\left|I_{f1}-I_{f2}\right|^2 \le \overline{H}_2\left|I_{f1}-I_{f2}\right|^2,\\ \left|A_3(t,I_{h1})-A_3(t,I_{h2})\right| &\le \frac{3}{2}p_3^2|I_{h1}-I_{h2}|^2 \le \overline{H}_3|I_{h1}-I_{h2}|^2,\\ \left|A_4(t,I_{m1})-A_4(t,I_{m2})\right| &\le \frac{3}{2}p_4^2|I_{m1}-I_{m2}|^2 \le \overline{H}_4|I_{m1}-I_{m2}|^2,\\ \left|A_5(t,I_{fh1})-A_5(t,I_{fh2})\right| &\le \frac{3}{2}p_5^2\left|I_{fh1}-I_{fh2}\right|^2 \le \overline{H}_5\left|I_{fh1}-I_{fh2}\right|^2,\\ \left|A_6(t,T_{fh1})-A_6(t,T_{fh2})\right| &\le \frac{3}{2}p_6^2\left|T_{fh1}-T_{fh2}\right|^2 \le \overline{H}_6\left|T_{fh1}-T_{fh2}\right|^2,\\ \left|A_7(t,R_{f1})-A_7(t,R_{f2})\right| &\le \frac{3}{2}p_7^2\left|R_{f1}-R_{f2}\right|^2 \le \overline{H}_7\left|R_{f1}-R_{f2}\right|^2,\\ \left|A_8(t,S_{v1})-A_8(t,S_{v2})\right| &\le \frac{3}{2}p_8^2|S_{v1}-S_{v2}|^2 \le \overline{H}_8|S_{v1}-S_{v2}|^2,\\ \left|A_9(t,I_{v1})-A_9(t,I_{v2})\right| &\le \frac{3}{2}p_9^2|I_{v1}-I_{v2}|^2 \le \overline{H}_9|I_{v1}-I_{v2}|^2. \end{aligned} \tag{45}$$

Therefore, in the event that their growing situation is such that:

$$\max\left\{\begin{array}{l}\dfrac{\beta_1^{\tau 2}\|I_v^2\|_\infty+\beta_2^{\tau 2}\|I_h^2\|_\infty+\beta_3^{\tau 2}\|I_{fh}^2\|_\infty+\mu_h^{\tau 2}}{\Lambda_h^{\tau 2}},\\ \dfrac{\delta_2^{\tau 2}\|I_h^2\|_\infty+(\sigma^\tau+\mu_h^\tau)^2}{\beta_1^{\tau 2}\|S_h^2\|_\infty\|I_v^2\|_\infty}|I_f|^2,\\ \dfrac{\delta_1^{\tau 2}\|I_f^2\|_\infty+(\varpi_h^\tau+\mu_h^\tau)^2}{\beta_2^{\tau 2}\|S_h^2\|_\infty}|I_h|^2,\\ \dfrac{\mu_h^{\tau 2}}{\varpi_h^{\tau 2}\|I_h^2\|_\infty}|I_m|^2,\\ \dfrac{\beta_3^{\tau 2}\|S_h^2\|_\infty+(\varpi_c^\tau+\mu_h^\tau)^2}{2(\delta_1^{\tau 2}\|S_h^2\|_\infty\|I_h^2\|_\infty+\delta_2^{\tau 2}\|I_f^2\|_\infty\|I_h^2\|_\infty)}|I_{fh}|^2,\\ \dfrac{\mu_h^{\tau 2}}{\varpi_c^{\tau 2}\|I_{fh}^2\|_\infty}|T_{fh}|^2,\\ \dfrac{\mu_h^{\tau 2}}{\sigma^{\tau 2}\|I_f^2\|_\infty}|R_f|^2,\\ \dfrac{\beta_v^{\tau 2}\|I_f^2\|_\infty+\mu_v^{\tau 2}}{\Lambda_v^{\tau 2}}|S_v|^2,\\ \dfrac{\mu_v^{\tau 2}}{\beta_v^{\tau 2}\|S_v^2\|_\infty\|I_v^2\|_\infty}|I_v|^2\end{array}\right\}\leq 1.$$

then a unique solution exists for the model system.

4. NUMERICAL SIMULATION

In this section, we numerically solve model 1. The following parameter values were considered in the numerical stimulation

$$\Lambda_h=0.9,\quad \Lambda_v=0.8,\quad \beta_1=0.0009,\quad \beta_2=0.0008,\quad \beta_3=0.0008,$$

$$\beta_v=0.008,\quad \delta_1=0.005,\quad \delta_2=0.09,\quad \sigma=0.05,\quad \varpi_h=0.9,$$

$$\varpi_c=0.09,\quad \mu_h=0.006,\quad \mu_v=0.060.$$

with the initial conditions:

$$S_h=100,\ I_f=10,\ I_h=10,\ I_{fh}=8,\ I_m=5,\ T_{fh}=5,\ R_f=10,\ S_v=50,\ I_v=5;$$

with time $t \in [0, 20]$ and time step $\Delta t = 0.025$.

We investigate five distinct values of the fractional order τ, each selected to examine its influence on the five infectious human compartments within model 1.

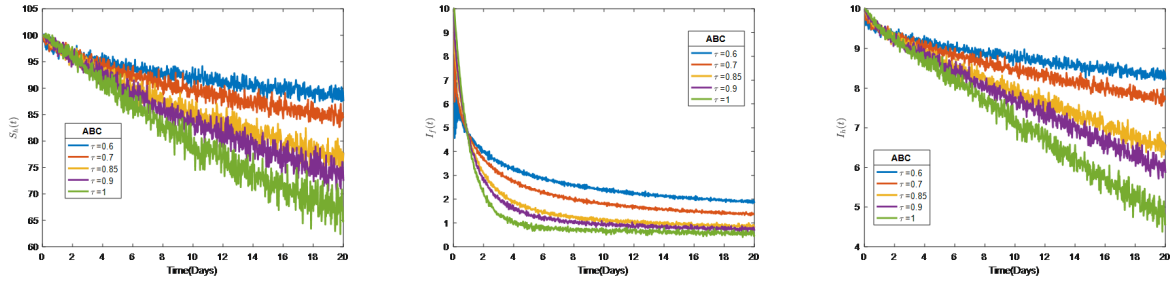

(A) (B) (C)

FIGURE 2

Figures 2a, 2b and 2c depict the dynamics of the susceptible humans $S_h(t)$, the infected humans with filariasis $I_f(t)$, and the infected humans with HIV/AIDS $I_h(t)$, respectively, under various values of the fractional order τ connected to the Atangana–Baleanu Caputo derivative. The findings show that the fractional order, which reflects the role of memory and genetic factors in the transmission process, has a quantifiable impact on the course of the disease.

Figure 2aillustrates that, as the fractional order increases towards 1 ($\tau = 1$), the number of susceptible decreases with vast fluctuations, which depicts that it is difficult to predict the dynamics in the community. This suggests that adding fractional-order effects slows down the depletion of the susceptible class by lowering the effective force of infection. This behavior is biologically consistent with systems where delayed immune response, behavioral adaptation, or environmental feedback reduces the spread of illness.

The filariasis-infected population initially increased sharply before gradually declining, as seen in Figure 2b. In the conventional framework, the decline is steeper for larger τ, suggesting that infections clear more quickly because of treatment influence or faster passage through the infection cycle. The decay becomes more gradual as τ is decreased, indicating a longer duration of filarial infection in the population. This is consistent with clinical evidence that filariasis infections are persistent, take a long time to resolve, and are significantly impacted by long-term immunological interactions, a characteristic that is better represented in fractional-order

systems. After day five, the distance between curves increases, suggesting that memory effects are not limited to the early stages but rather compound over time.

The HIV-infected class likewise gradually declines in Figure 2c, albeit more slowly than $I_f(t)$, which is in line with the fact that HIV infection is chronic. The rate of decline increases as τ increases, just like in the earlier subfigures. The fractional cases ($\tau < 1$) capture realistic delays in ART commencement, immune suppression progression, and viral clearance response by maintaining greater infection levels for a longer period of time. The outcome confirms that when memory affects treatment adherence history, viral latency, and immune exhaustion are disregarded, integer-order models may understate the durability of HIV infections.

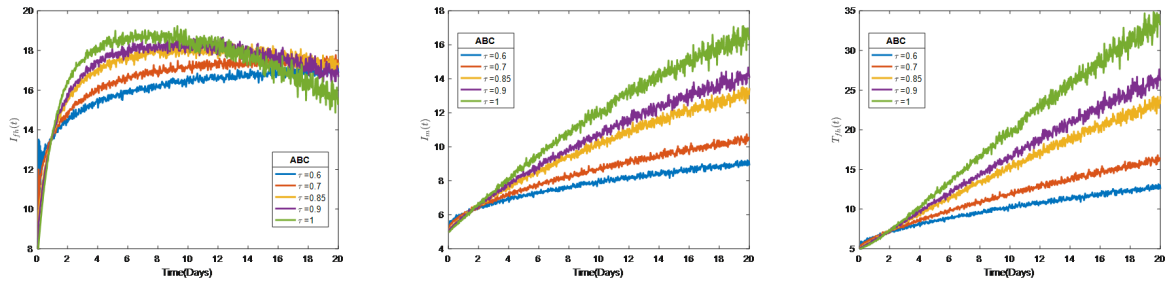

(A) (B) (C)

FIGURE 3

Figures 3a, 3b, and 3c show the dynamics of the co-infection humans $I_{fh}(t)$, the managed HIV infected humans $I_m(t)$, and the treated co-infected $T_{fh}(t)$, respectively.

In Figure 3a, I_{fh} exhibits a sharp increase followed by a stabilization period, reaching greater levels as the fractional order rises. While lesser τ values delay and lower the saturation threshold, the classical situation ($\tau = 1$) has the highest peak and final burden of co-infection. This behavior demonstrates the moderating effect of memory: the accumulation of co-infected individuals is slower the longer previous infection states have an impact on current transmission. The outcome is in line with clinical reality, which shows that filarial illness usually progresses slowly but is much worse in immunocompromised hosts.

In contrast to a typical HIV-infected compartment, $I_m(t)$ stands for people undergoing antiretroviral therapy (ART) or HIV treatment. For all fractional orders, the size of this class

grows gradually over time in Figure 3b. However, τ has a significant impact on the rate of entrance into management: smaller τ values result in a slower climb, whereas the classical model forecasts the largest and fastest accumulation. This is a reflection of actual delays in HIV care enrollment, such as delayed diagnosis, unequal access, difficulties with adherence, or delayed ART initiation. Because of its intrinsic memory structure, the fractional model reflects these delays, suggesting that integer-order models might overestimate the effectiveness and rate of HIV treatment scale-up in co-endemic areas.

With the same hierarchical ordering of curves by τ, Figure 3c illustrates how the population undergoing treatment for both infections increases with time. Lower τ values hinder the shift into dual therapy, while the greatest values once more appear in the classical scenario. This finding supports the notion that co-infected patients must overcome extra obstacles prior to getting combined therapy, including clinical diagnosis of infections, drug compatibility problems, comorbidity effects, and health-system constraints. Ignoring memory effects could result in an overestimation of treatment coverage and, consequently, an unrealistic forecast of programmatic success, as indicated by the growing gap between $\tau = 1$ and $\tau < 1$ over time.

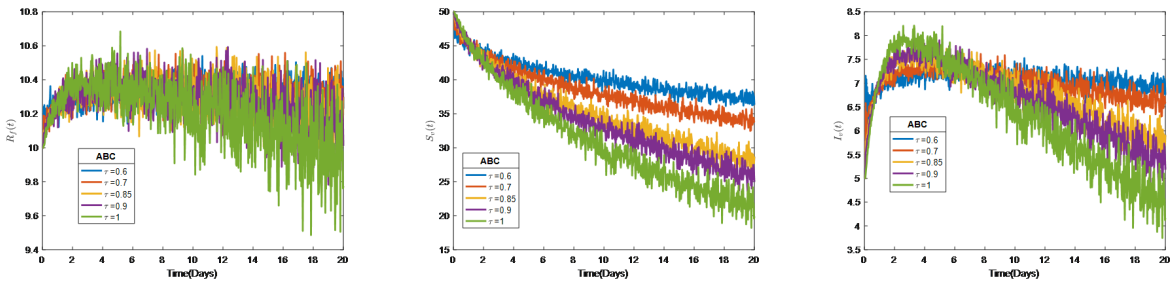

(A) (B) (C)

FIGURE 4

Figures 4a, 4b, and 4c show the dynamics of the recovered from filariasis infected humans $R_f(t)$, the susceptible insects $S_v(t)$, and the infected vector $I_v(t)$, respectively.

Figure 4a reflects the accumulation of people recovering from filariasis infection and initially rises in the early phases of the simulation. For all values of τ, Figure 4c shows an initial growth phase followed by a slow fall. When the system acts more like the traditional integer-order model, higher fractional orders (e.g., $\tau = 1$) result in a sharper climb and earlier peak,

suggesting a faster rate of recovery. Conversely, a delayed and smoother peak is linked to lower fractional orders (e.g., $\tau = 0.6$), indicating that the recovery response is slowed by stronger memory effects. This behavior suggests that human recovery dynamics are delayed because the fractional-order term captures residual impacts of previous infection levels. The numerical simulation's incorporated stochastic effects could be the cause of the variations seen around the paths.

As a result of ongoing exposure to infectious human hosts, the vulnerable mosquito compartment decreases monotonically over the course of the simulation. The fractional order τ has a significant impact on the pace of depletion; lower values result in a sharper fall. This suggests that the transmission process quickens and turns susceptible mosquitoes into infected ones more quickly when memory effects are more noticeable. On the other hand, when τ gets closer to 1, the decrease in Figure 4b becomes less hostile, indicating a slower rate of infection. These results highlight how the fractional derivative affects the vector population's transmission efficiency.

In Figure 4c, the rise-and-fall profile is distinctive; every simulation demonstrates an early rise in $I_v(t)$, then a gradual decline as the infection pressure drops. Once more, fractional-order effects are important: larger τ values result in more gradual increases with lower peak intensities, whereas lower τ values create stronger and earlier epidemic peaks. This behavior is in line with the scientific hypothesis that when memory effects are dominant, there will be a stronger infection force and a faster host-vector cycle. All curves eventually decline, indicating that vector infection decreases with time as a result of either host recovery, vector mortality, or a reduction in the number of mosquitoes that are susceptible. The ordering of curves indicates once more that the rate of infection dissemination and persistence within the vector population is controlled by the fractional index τ: higher τ results in milder but longer-lasting transmission, while lower τ causes more severe but brief infection peaks.

5. Fractional Optimal Control Problem

In this section, the control parameters $u_i(t)$ are included in the model to explore the effort designed to bring about prevention of the spread of filariasis, HIV, as well as filariasis–HIV co-infection. For consistency, the controls are numbered from u_1 to u_5:

- $u_1(t)$: vector control (example, insecticide spraying, environmental management).
- $u_2(t)$: prevention of filariasis (example, bed nets, health education).
- $u_3(t)$: prevention of HIV (example, safe sex practices, PrEP).
- $u_4(t)$: treatment for filariasis-infected individuals.
- $u_5(t)$: treatment for HIV-infected and co-infected individuals.

Each control satisfies:

$$0 \leq u_i(t) \leq 1, \quad i = 1,2,3,4,5.$$

After adding the control variables to system 1, we obtain the control system:

$$\begin{aligned}
{}_0^{ABC}D^{\tau}S_h &= \Lambda_h - \beta_1(1-u_2)S_hI_v - \beta_2(1-u_3)S_hI_h - \beta_3(1-u_5)S_hI_{fh} - \mu_hS_h,\\
{}_0^{ABC}D^{\tau}I_f &= \beta_1(1-u_2)S_hI_v - (\sigma+\mu_h)I_f - \delta_2I_fI_h - u_4I_f,\\
{}_0^{ABC}D^{\tau}I_h &= \beta_2(1-u_3)S_hI_h - \delta_1I_hI_f - (\mu_h+\varpi_h)I_h - u_5I_h,\\
{}_0^{ABC}D^{\tau}I_{fh} &= \beta_3(1-u_5)S_hI_{fh} + \delta_2I_fI_h + \delta_1I_hI_f - (\mu_h+\varpi_c)I_{fh} - u_5I_{fh},\\
{}_0^{ABC}D^{\tau}I_m &= \varpi_hI_h - \mu_hI_m + u_5I_h,\\
{}_0^{ABC}D^{\tau}T_{fh} &= \varpi_cI_{fh} - \mu_hT_{fh} + u_5I_{fh},\\
{}_0^{ABC}D^{\tau}R_f &= \sigma I_f - \mu_hR_f + u_4I_f,\\
{}_0^{ABC}D^{\tau}S_v &= \Lambda_v - \beta_v(1-u_1)S_vI_f - \mu_vS_v,\\
{}_0^{ABC}D^{\tau}I_v &= \beta_v(1-u_1)S_vI_f - \mu_vI_v
\end{aligned} \tag{46}$$

under non-negative initial conditions.

The objective functional for system 46 is:

$$J(u_1,u_2,u_3,u_4,u_5) = \int_0^{t_f}\left[c_1I_f + c_2I_h + c_3I_m + c_4I_{fh} + c_5I_v + W_1u_1^2 + W_2u_2^2 + W_3u_3^2 + W_4u_4^2 + W_5u_5^2\right]dt. \tag{47}$$

The main emphasis of our control problem is the quantity of HIV infected humans, the vector, filariasis infected humans and coin-infected humans, as well as the related expenses for prevention and treatment controls that are subject to the control system 46 that includes $u_1(t)$, $u_2(t)$, $u_3(t)$, $u_4(t)$, and $u_5(t)$. The coefficients, c_i for $i = 1,..4$, and W_i for $i = 1,\ldots,5$ in line with

the scales and the importance of the nine components included in objective functional, indicate weight and the balancing cost elements, while t_f represents the end time.

The goal is to have an ideal control, u_1, u_2, u_3, u_4, and u_5^* such that $\mathscr{U} = \{(u_1, u_2, u_3, u_4, u_5)\}$, so that u_1, u_2, u_3, u_4, u_5 are measurable with $0 \leq u_1 \leq 1$, $0 \leq u_2 \leq 1$, $0 \leq u_3 \leq g_2$, $0 \leq u_4 \leq g_3$, and $0 \leq u_5 \leq g_3$, for $t \in [0, t_f]$. Lebesgue integrable functions with bounded functions are presumed to be the control functions provided by $u_1(t)$, $u_2(t)$, $u_3(t)$, $u_4(t)$, and $u_5(t)$. System 47 specifies the following five recommended controls: $u_1(t)$ is the vector control, whereas the efforts to prevent HIV and filariasis infections are indicated by the controls, $u_2(t)$ and $u_3(t)$. The fourth regulation filariasis treatment is indicated by $u_4(t)$, where $0 \leqslant u_4 \leqslant g_2$, where g_2 indicates the effectiveness of the medication used to treat filariasis patients. The treatment of HIV infected humans and co-infected humans is demonstrated by the control $u_5(t)$, which is intended to serve HIV infected humans and co-infected humans and fulfills $0 \leqslant u_5 \leqslant g_3$, where g_3 indicates the medicine effectiveness for HIV infected humans and co-infected patients. Here, g_3 indicates the drug efficacy utilized to treat HIV and filariasis co-infected individuals. The Pontryagin Maximum Principle, which originates from 47, is the essential requirement that an ideal solution must meet. This idea transforms equation 46 and 47into a type considered as a problem that involves minimizing a Hamiltonian H pointwise while taking into account the controls u_1, u_2, u_3, u_4, and u_5. We define the Hamiltonian by using the adjoint variables with respect to 48 as indicated by N_i.

$$
\begin{aligned}
H = {} & c_1 I_f + c_2 I_h + c_3 I_m + c_4 I_{fh} + c_5 I_v + W_1 u_1^2 + W_2 u_2^2 + W_3 u_3^2 + W_4 u_4^2 + W_5 u_5^2 \\
& + N_1 \left(\Lambda_h - \beta_1 (1-u_2) S_h I_v - \beta_2 (1-u_3) S_h I_h - \beta_3 (1-u_5) S_h I_{fh} - \mu_h S_h \right) \\
& + N_2 \left(\beta_1 (1-u_2) S_h I_v - \sigma I_f - \delta_2 I_f I_h - \mu_h I_f - u_4 I_f \right) \\
& + N_3 \left(\beta_2 (1-u_3) S_h I_h - \delta_1 I_h I_f - \mu_h I_h - \varpi_h I_h - u_5 I_h \right) \\
& + N_4 \left(\beta_3 (1-u_5) S_h I_{fh} + \delta_2 I_f I_h + \delta_1 I_h I_f - \mu_h I_{fh} - \varpi_c I_{fh} - u_5 I_{fh} \right) \\
& + N_5 \left(\varpi_h I_h - \mu_h I_m + u_5 I_h \right) \\
& + N_6 \left(\varpi_c I_{fh} - \mu_h T_{fh} + u_5 I_{fh} \right) \\
& + N_7 \left(\sigma I_f - \mu_h R_f + u_4 I_f \right)
\end{aligned}
$$

$$+N_8\left(\Lambda_v-\beta_v(1-u_1)S_vI_f-\mu_vS_v\right)$$

$$+N_9\left(\beta_v(1-u_1)S_vI_f-\mu_vI_v\right). \tag{48}$$

Where N_{S_h}, N_{I_f}, N_{I_h}, N_{I_m}, $N_{I_{fh}}$, $N_{T_{fh}}$, N_{R_f}, N_{S_v} and N_{I_v} indicates the adjoint variables or the co-state. It is possible to construct the system of adjoint equations by applying the proper partial differentiations of the equation 48 of Hamiltonian with regard to the state variables.

Theorem 2. The optimal controls given by $u_1(t)$, $u_2(t)$, $u_3(t)$, $u_4(t)$, $u_5(t)$ and it's solutions N_{S_h}, N_{I_f}, N_{I_h}, N_{I_m}, $N_{I_{fh}}$, $N_{T_{fh}}$, N_{R_f}, N_{S_v} and N_{I_v} of the equations given by 46- 47 minimizing $J(u_1,u_2,u_3,u_4,u_5)$ over $\mathscr{U}$, hence, the adjoint variables given by N_{S_h}, N_{I_f}, N_{I_h}, N_{I_m}, $N_{I_{fh}}$, $N_{T_{fh}}$, N_{R_f}, N_{S_v} and N_{I_v} exist and satisfies:

$$-\frac{dN_i}{dt}=\frac{\partial H}{\partial i} \tag{49}$$

where $i=N_{S_h},N_{I_f},N_{I_h},N_{I_m},N_{I_{fh}},N_{T_{fh}},N_{R_f},N_{S_v},N_{I_v}$ as well as the prerequisites of transversality:

$$N_{S_h}(t_f)=N_{I_f}(t_f)=N_{I_h}(t_f)=N_{I_m}(t_f)=N_{I_{fh}}(t_f)=N_{T_{fh}}(t_f)=N_{R_f}(t_f)=0,$$

$$N_{S_v}(t_f)=N_{I_v}(t_f)=0.$$

and the optimal control characterization:

$$u_i^*=\min\Big(\max(0,(\lambda_iC_i)/2),1\Big),\quad i=1,2,3,4,5,$$

Where $\lambda_i(t)$ are the adjoint variables C_i are the control weight parameters $0\le u_i\le 1$ ensures biological feasibility.

$$u_1^*=\min\left(\max\left(0,\frac{-(2\omega_8)/a_8X_8(T)E_\tau(-a_8(T-t)^\tau\beta_vS_v)}{2C_1}\right),1\right)$$

$$u_2^*=\min\left(\max\left(0,\frac{-(2\omega_1)/a_1X_1(T)E_\tau(-a(T-t)^\tau\beta_1S_hI_v)-(-(2w_2)/a_2X_2(T)E_\tau(-a_2(T-t)^\tau\beta_1I_v))}{2C_2}\right),1\right)$$

$$u_3^*=\min\left(\max\left(0,\frac{-(2\omega_1)/a_1X_1(T)E_\tau(-a(T-t)^\tau\beta_2S_hI_h)-(-(2w_3)/a_3X_3(T)E_\tau(-a_3(T-t)^\tau\beta_2I_h)}{2C_3}\right),1\right)$$

$$u_4^*=\min\left(\max\left(0,\frac{-(2w_2)/a_2X_2(T)E_\tau(-a_2(T-t)^\tau)I_f}{2C_4}\right),1\right)$$

$$u_5^*=\min\left(\max\left(0,\frac{-(2w_3)/a_3X_3(T)E_\tau(-a_3(T-t)^\tau I_h+(-(2\omega_4)/a_4X_4(T)E_\tau(-a_4(T-t)^\tau I_v)}{2C_5}\right),1\right) \tag{50}$$

Proof: With respect to the controls u_1, u_2, u_3, u_4, and u_5, the convexity of the integrand of J establishes the existence of the system of an optimal control, as shown by Corollary 4.1 of 50, between the state variables and the Lipschitz property of the state system and the state solutions. In order to produce the system of adjoint variables, the Hamiltonian equation must be differentiated with the proper state variables of the control system and the optimality system. The system of adjoint equations can be obtained by computing and rearranging

$$
\begin{aligned}
{}_0^{ABC}D^{-\tau}\lambda_1 &= \lambda_1(\beta_1(1-u_2)I_v+\beta_2(1–u_3)I_h+\beta_3 I_c+\mu_h)–\lambda_2\beta_1(1-u_2)I_v–\lambda_3\beta_2(1–u_3)I_h–\lambda_4\beta_3 I_{fh}\\
{}_0^{ABC}D^{-\tau}\lambda_2 &= 2\omega_1 I_f+\lambda_2(\sigma+\mu+u_4+\delta_2 I_h)-\lambda_4\delta_2 I_h–\lambda_7\sigma–\lambda_8\beta_v(1-u_1)S_v\\
{}_0^{ABC}D^{-\tau}\lambda_3 &= 2\omega_2 I_h+\lambda_3(\varpi_h+\mu+u_5+\delta_1 I_f)–\lambda_4\delta_1 I_f–\lambda_5\varpi_h\\
0^{ABC}D^{-\tau}\lambda_4 &= 2\omega_3 Ifh+\lambda_4(\varpi_c+\mu+u_5)–\lambda_6\varpi_c\\
{}_0^{ABC}D^{-\tau}\lambda_5 &= 2\omega_4 I_m+\lambda_5\mu_h \quad (9)\\
0^{ABC}D^{-\tau}\lambda_6 &= 2\omega_5 Tfh+\lambda_6\mu_h\\
{}_0^{ABC}D^{-\tau}\lambda_7 &= \lambda_7\mu_h\\
{}_0^{ABC}D^{-\tau}\lambda_8 &= \lambda_8(\beta_v(1–u_1)I_f+\mu_v)\\
{}_0^{ABC}D^{-\tau}\lambda_9 &= \lambda_9\mu_v–\lambda_1\beta_1(1–u_2)S_h. \qquad (51)
\end{aligned}
$$

With the boundary conditions $\lambda_i(t_f)=0$, where $i=1,2,3,\ldots,9$.

When the restrictions and optimal control characterisation values u_i^* for $i=1,\ldots,5$ are calculated, the outcome displayed in the optimal control characterization will be obtained, and the following can be acquired:

$$
\begin{aligned}
0=\frac{\partial H}{\partial u_1} &= 2C_1+\frac{-(2\omega_8)/a_8X_8(T)E_\tau(-a_8(T-t)^\tau\beta_v S_v)}{1},\\
0=\frac{\partial H}{\partial u_2} &= 2C_2+\frac{-(2\omega_1)/a_1X_1(T)E_\tau(-a(T-t)^\tau\beta_1 S_h I_v)-(-(2w_2)/a_2X_2(T)E_\tau(-a_2(T-t)^\tau\beta_1 I_v))}{1},\\
0=\frac{\partial H}{\partial u_3} &= 2C_3+\frac{-(2\omega_1)/a_1X_1(T)E_\tau(-a(T-t)^\tau\beta_2 S_h I_h)-(-(2w_3)/a_3X_3(T)E_\tau(-a_3(T-t)^\tau\beta_2 I_h)}{1},\\
0=\frac{\partial H}{\partial u_4} &= 2C_4+\frac{-(2w_2)/a_2X_2(T)E_\tau(-a_2(T-t)^\tau)I_f}{1},\\
0=\frac{\partial H}{\partial u_5} &= 2C_5+\frac{-(2w_3)/a_3X_3(T)E_\tau(-a_3(T-t)^\tau I_h+(-(2\omega_4)/a_4X_4(T)E_\tau(-a_4(T-t)^\tau I_v)}{1}. \qquad (52)
\end{aligned}
$$

Thus, we have, for instance, [25].

$$u_1^* = \frac{-(2\omega_8)/a_8 X_8(T) E_\tau(-a_8(T-t)^\tau \beta_v S_v)}{2C_1},$$

$$u_2^* = \frac{-(2\omega_1)/a_1 X_1(T) E_\tau(-a(T-t)^\tau \beta_1 S_h I_v) - (-(2w_2)/a_2 X_2(T) E_\tau(-a_2(T-t)^\tau \beta_1 I_v))}{2C_2},$$

$$u_3^* = \frac{-(2\omega_1)/a_1 X_1(T) E_\tau(-a(T-t)^\tau \beta_2 S_h I_h) - (-(2w_3)/a_3 X_3(T) E_\tau(-a_3(T-t)^\tau \beta_2 I_h)}{2C_3},$$

$$u_4^* = \frac{-(2w_2)/a_2 X_2(T) E_\tau(-a_2(T-t)^\tau) I_f}{2C_4},$$

$$u_5^* = \frac{-(2w_3)/a_3 X_3(T) E_\tau(-a_3(T-t)^\tau I_h + (-(2\omega_4)/a_4 X_4(T) E_\tau(-a_4(T-t)^\tau I_v)}{2C_5}. \tag{53}$$

The following is a summary of how the standard control arguments that explain about with controls boundaries are used:

$$u_i^* = \begin{cases} 0 & \text{if } \xi_i^* \le 0 \\ \xi_i^* & \text{if } 0 \le \xi_i^* \le 1 \\ 1 & \text{if } \xi_i^* \ge 1 \end{cases},$$

Whereas $i \in \{1,2,3,4,5\}$ And:

$$\xi_1^* = \frac{-(2\omega_8)/a_8 X_8(T) E_\tau(-a_8(T-t)^\tau \beta_v S_v)}{2C_1},$$

$$\xi_2^* = \frac{-(2\omega_1)/a_1 X_1(T) E_\tau(-a(T-t)^\tau \beta_1 S_h I_v) - (-(2w_2)/a_2 X_2(T) E_\tau(-a_2(T-t)^\tau \beta_1 I_v))}{2C_2},$$

$$\xi_3^* = \frac{-(2\omega_1)/a_1 X_1(T) E_\tau(-a(T-t)^\tau \beta_2 S_h I_h) - (-(2w_3)/a_3 X_3(T) E_\tau(-a_3(T-t)^\tau \beta_2 I_h)}{2C_3},$$

$$\xi_4^* = \frac{-(2w_2)/a_2 X_2(T) E_\tau(-a_2(T-t)^\tau) I_f}{2C_4},$$

$$\xi_5^* = \frac{-(2w_3)/a_3 X_3(T) E_\tau(-a_3(T-t)^\tau I_h + (-(2\omega_4)/a_4 X_4(T) E_\tau(-a_4(T-t)^\tau I_v)}{2C_5}. \tag{54}$$

6. Numerical Stimulation of the Control System

Detailed numerical solution of the control system is provided below, along with the system without controls and optimal control characterization. The solution would be displayed as graphical results.A set of controls combinations and numerical solutions would be provided

in details. The numerical results would be computed by the software MATLAB. The adjoint system, controls characterization, and control system would all be solved numerically, and the results would be displayed graphically. The optimal control solution would be obtained by calculating the optimality system, which consists of the adjoint system and the state system. In order to determine the system control solution, the solution with control is represented by a bold blue line, and the solution without control is depicted using a dashed red line. The following parameter values were used

$$\Lambda_h = 0.9, \quad \Lambda_v = 0.8, \quad \beta_1 = 0.0009, \quad \beta_2 = 0.0008, \quad \beta_3 = 0.0008,$$
$$\beta_v = 0.008, \quad \delta_1 = 0.005, \quad \delta_2 = 0.09, \quad \sigma = 0.05, \quad \varpi_h = 0.9,$$
$$\varpi_c = 0.09, \quad \mu_h = 0.006, \quad \mu_v = 0.060,$$

with the initial conditions:

$$X(0) = 0,$$

and the objective functional weight:

$$A_1 = 1\ A_2 = 1\ A_3 = 1\ A_4 = 1\ A_5 = 1$$

And Control weights:

$$B_1 = 20\ B_2 = 30\ B_3 = 50\ B_4 = 20\ B_5 = 10$$

The following results were achieved:

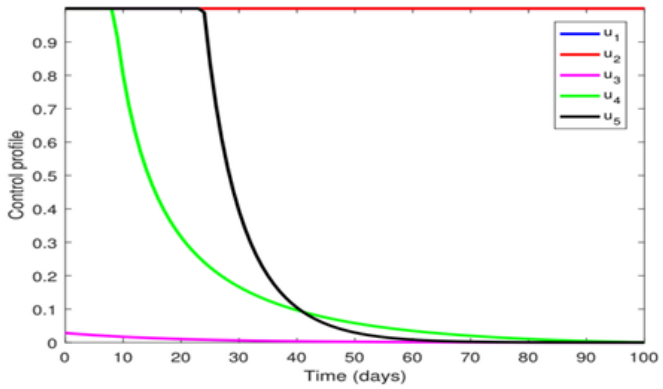

FIGURE 5

In order to achieve a desired system response, the graph's control profile shows how various control inputs (u_1, u_2, u_3, u_4, and u_5) change over time (days) as seen in figure 5. Phased control efforts can efficiently manage complex systems while optimizing resource utilization, as the control profile emphasizes, underscoring the significance of strategic intervention planning.

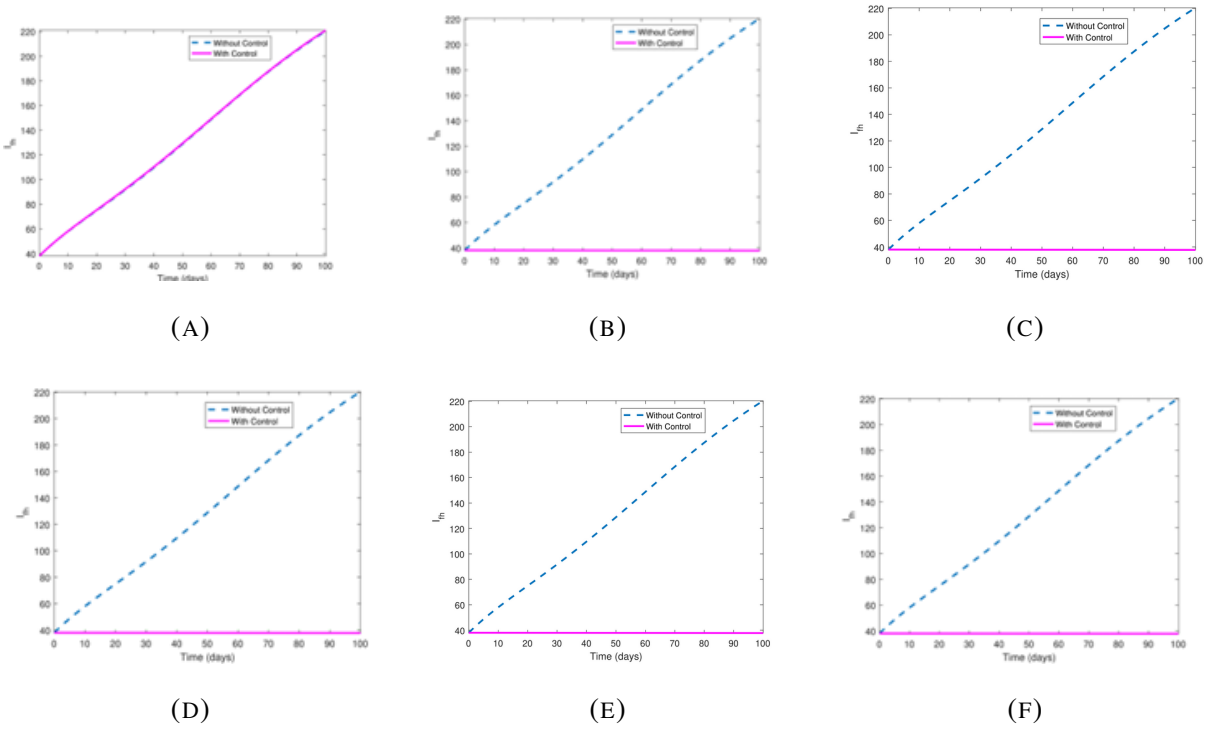

(A) (B) (C)

(D) (E) (F)

FIGURE 6

The temporal evolution of the filariasis-HIV co-infected human compartments during a 100-day simulation period is shown in Figures 6a–6f, which compare two scenarios: the absence of control (blue dashed line) and the presence of control (magenta line). In order to reduce the transmission and co-infection burden of filariasis in the presence of HIV, a combination of intervention approaches, including treatment, prevention, and vector management methods, have been put into place.

These results highlight the significance of integrated management tactics in reducing the dual disease burden in co-endemic locations from a biological perspective. Preventive and treatment-based actions, such as mass drug administration, vector reduction, and early therapeutic care, can significantly lower the rate of new co-infections, as seen by the stark difference between the

"with control" and "without control" scenarios. Overall, the findings indicate that among populations at risk of HIV co-infection, a well-executed management strategy not only reduces the prevalence of co-infection but also improves the sustainability of disease elimination programs aimed at filariasis.

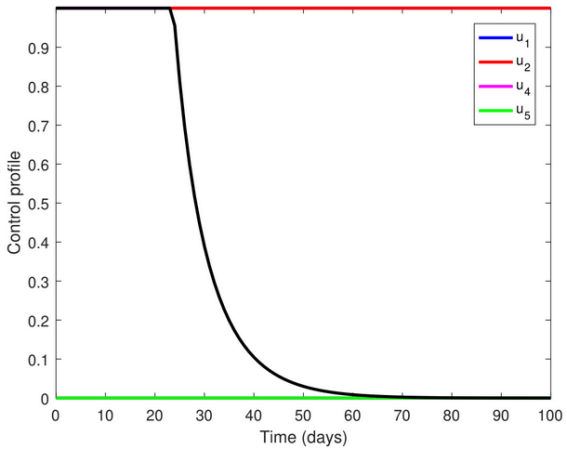

FIGURE 7

Figure 7 is the dynamics of the four control variables for the prevention and treatment of filariasis-infected humans. A multi-tiered intervention strategy is highlighted by the ideal control profiles: an ongoing backdrop prevention initiative a therapy attempt that was initially effective but eventually declined as well as a well-planned, aggressive campaign. Throughout the simulation, the control stays very low, suggesting that, given the specified cost and efficacy characteristics, this technique gives little additional value. In order to maintain long-term illness reduction, this integrated approach effectively suppresses both single and co-infections, reduces the danger of reinfection, and takes advantage of the memory-dependent dynamics of the fractional-order model. The findings emphasize that the best strategy for controlling and possibly eradicating filariasis in HIV-endemic areas is to combine consistent preventative measures with timely, enhanced therapies.

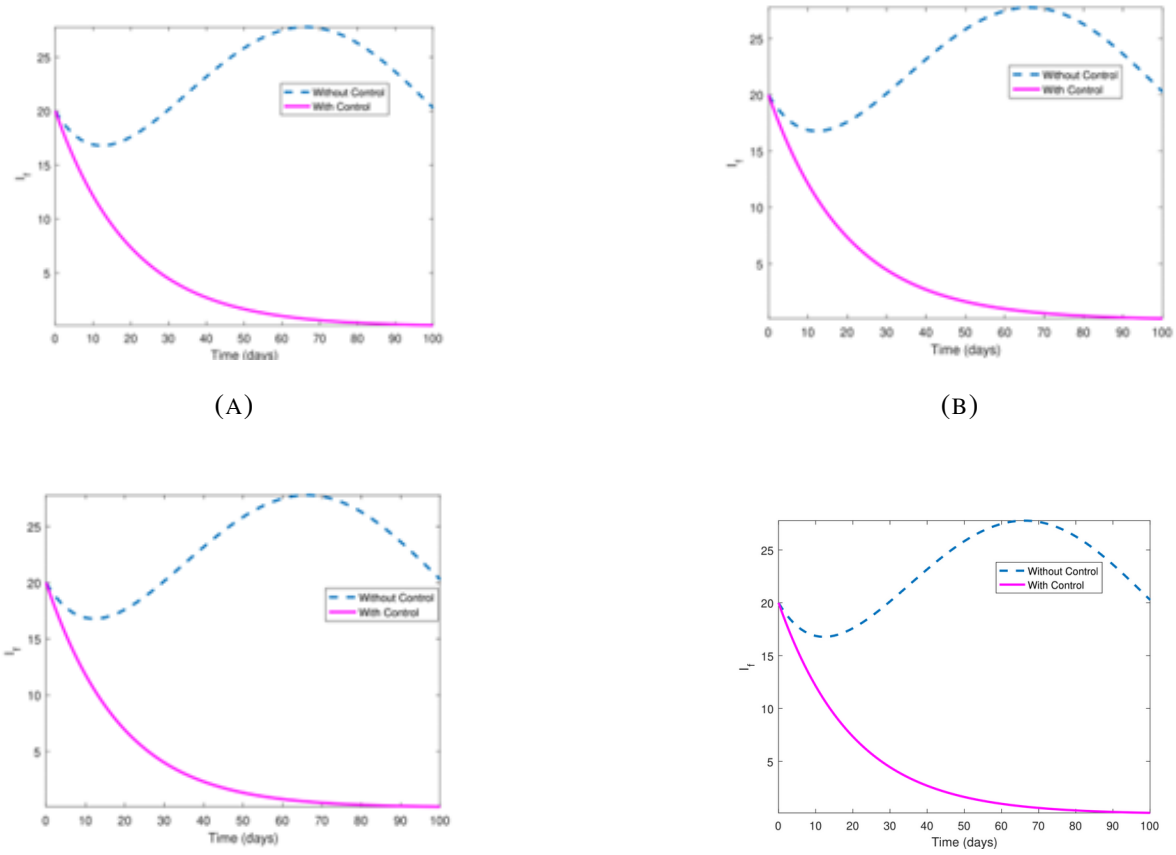

FIGURE 8

In figures 8a – 8d, the temporal dynamics offer strong proof of the effectiveness of control strategies in reducing the variable's intensity or spread, which is assumed to reflect an infectious burden or incidence rate. The "With Control" and "Without Control" scenarios' compared trajectories over a 100-day period show significant differences in results, highlighting the crucial impact of intervention techniques.

The blue dashed line, which shows a classical epidemic curve in the absence of control measures, has an initial rise, a prominent peak that exceeds 25 units, and a slow fall. This pattern is a sign of unregulated transmission, where the biological, social, or environmental system allows the occurrence to continue to spread. The peak points to a saturation point that may be caused by a lack of resources, changes in behavior, or a natural decline in the number of vulnerable people.

On the other hand, toward the end of the observation period, the "With Control" trajectory (magenta solid line) shows a monotonic reduction from the same initial condition, getting close to zero levels. This implies that the control measures that were put in place had a suppressive effect, probably via mechanisms like decreased vulnerability, improved recovery, or decreased contact rates. The lack of a peak and the consistent downward trend suggest that the control measures were timely and strong enough to stop the situation from getting worse.

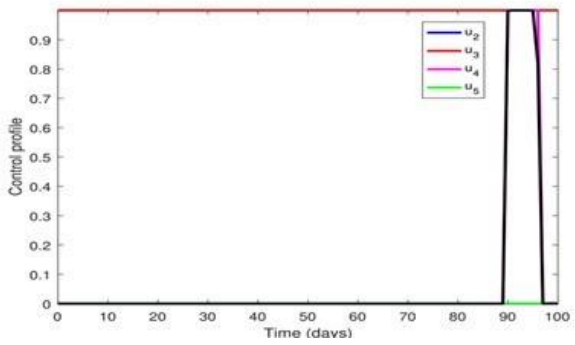

FIGURE 9

Figure 9 shows the four time-dependent controls $u_2(t)$, $u_3(t)$, $u_4(t)$, and $u_5(t)$ represent prevention and treatment measures aimed at various components of the HIV/AIDS and filariasis co-infection system. Their consequences are analyzed in relation to the dynamics of both HIV/AIDS and HIV-managed class transitions, as well as the interactions between filarial infection and HIV progression. The control profiles show that as the co-infection load increases, HIV/AIDS interventions become more crucial. The optimal strategy strategically postpones expensive HIV therapies until they achieve the greatest possible epidemiological impact. The abrupt activation of HIV-related controls near the end of the time horizon indicates that targeted, timely, and cost-effective implementation of antiretroviral therapy (ART) and prevention measures is essential to effectively suppress the HIV epidemic in a filariasis-endemic area—particularly during periods when co-infection feedback mechanisms amplify transmission potential.

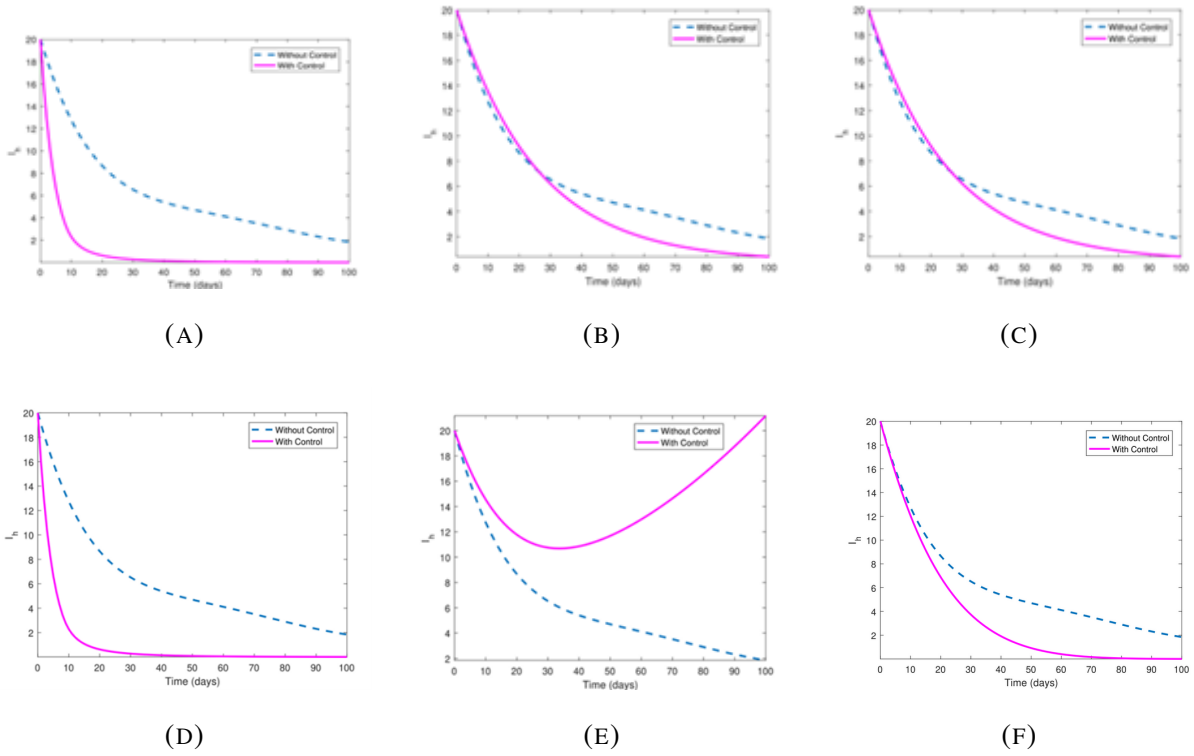

(A) (B) (C)

(D) (E) (F)

FIGURE 10

Those who actively carry the virus without receiving adequate care or treatment are represented by figure 10a – 10f. According to the model, this compartment tends to grow over time in the absence of intervention, suggesting continuing transmission, disease progression, and a persistent epidemic. This class's continuous expansion highlights the serious problem of untreated HIV infections, which significantly increase the infected pool and promote continued population spread.

The observed trends indicate that the percentage of HIV-positive people will either stay high or rise in the absence of focused initiatives, such as broad testing, early diagnosis, and care linkage, undermining control efforts. This increasing trend emphasizes how crucial it is to put policies in place that concentrate on lowering the number of new infections and raising the rate at which sick people are found and connected to treatment programs. Reducing overall prevalence and stopping the epidemic's momentum require addressing this compartment.

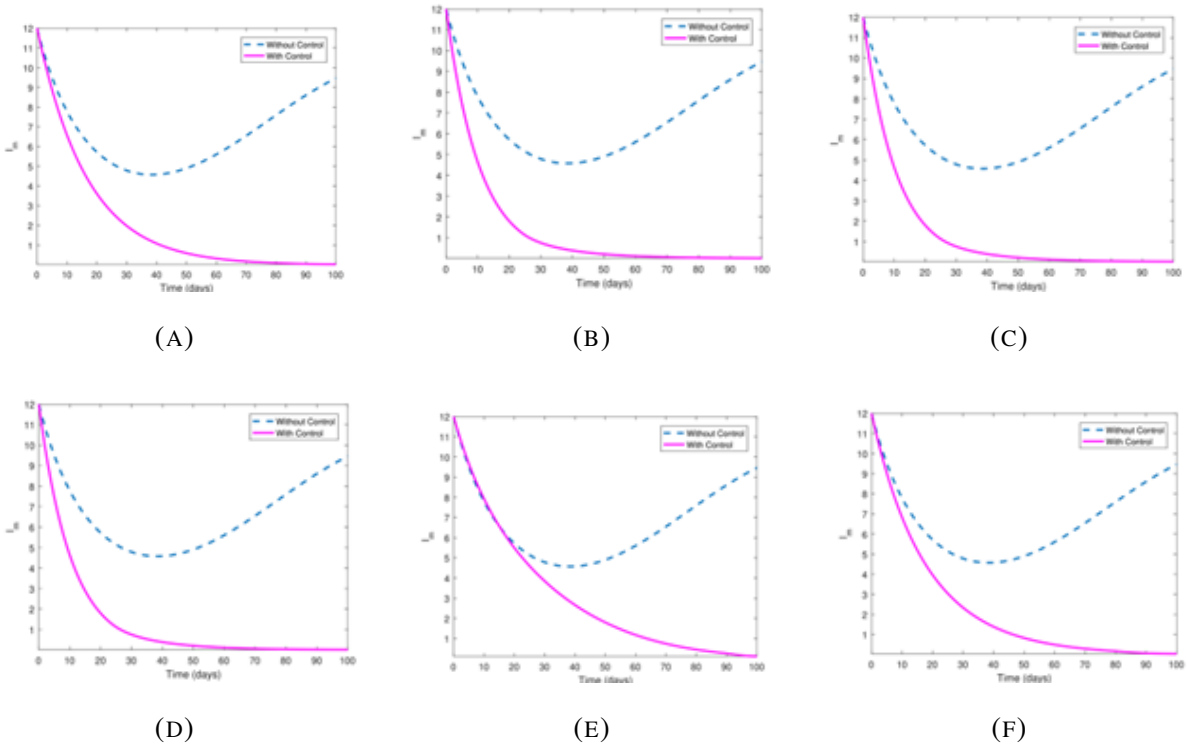

(A) (B) (C)

(D) (E) (F)

FIGURE 11

Figure 11a – 11f includes people undergoing treatment, primarily antiretroviral medication (ART), which is intended to inhibit viral replication and stop the disease from progressing. The model shows that the size of this compartment tends to stabilize or decrease over time given efficient management techniques. This suggests that HIV-positive people's infectiousness can be considerably reduced by treatment, which lowers the population's potential for transmission.

This class's dynamics highlight how important treatment coverage, adherence, and retention are. The overall infectious pool decreases as the percentage of people in the managed class rises, which aids in the control of epidemics. This compartment's stabilization or decrease demonstrates how well management techniques have changed the course of the pandemic. To optimize the effectiveness of treatment programs, it emphasizes the significance of ongoing healthcare interventions, enhanced accessibility, and adherence support.

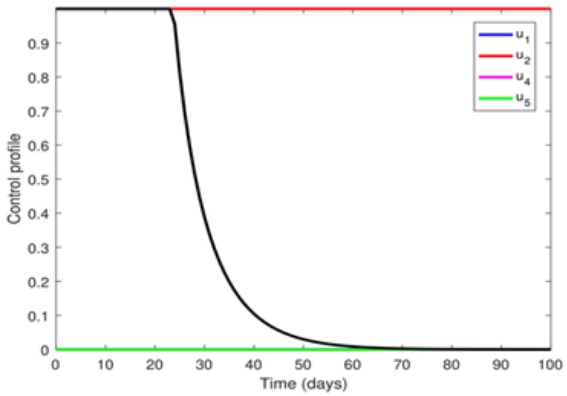

FIGURE 12

Figure 12 demonstrates that (vector control) stays at its greatest level for the duration of the time, suggesting that the best method for lowering filariasis transmission in the co-infection model is continuous, intense vector suppression. Because mosquito populations rebound quickly and any drop in vector control would allow the disease to resurface, this is biologically sensible, therapy of sick humans, or , is high at first but quickly declines after 30 to 40 days. This indicates that early vigorous therapy helps lower the human infectious reservoir, after which further treatment has no extra value. Because vector control reduces filariasis transmission more than HIV-related efforts, the other controls, , stay close to zero. Overall, the profile demonstrates that the best strategy for controlling filariasis–HIV co-infection in the model is to combine long-term vector management with brief early treatment attempts.

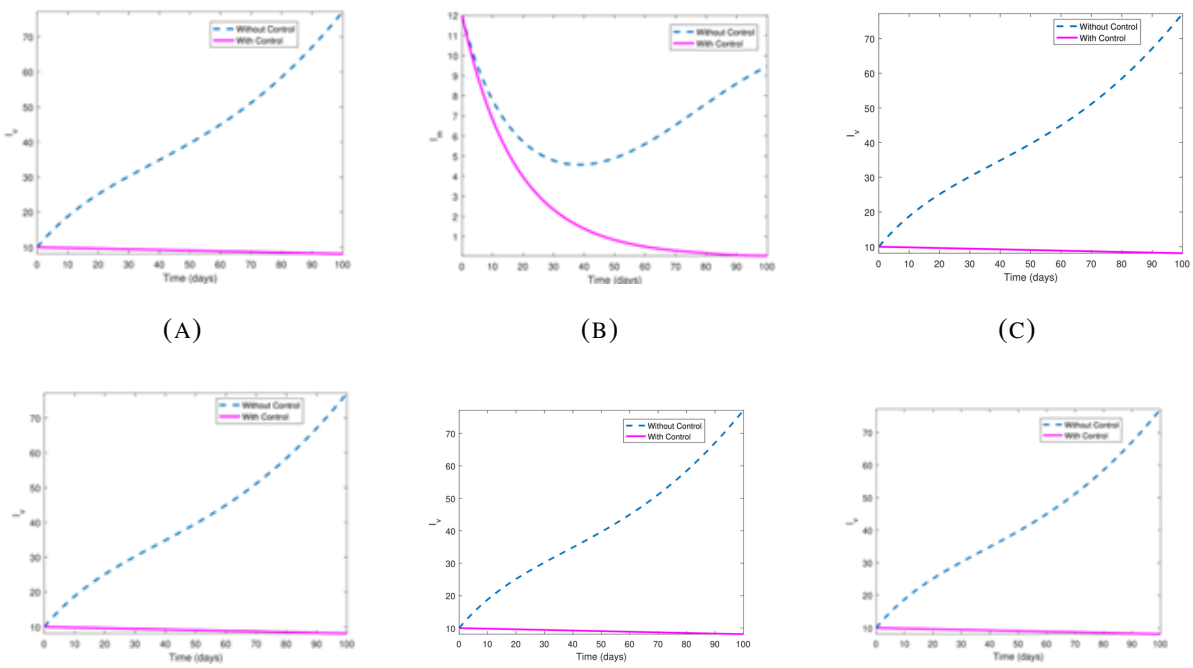

(A) (B) (C)

(D) (E) (F)

FIGURE 13

By comparing the trajectories seen under conditions with and without control interventions over a 100-day horizon Figure 13a – 13f clarify the temporal dynamics of infected-vector populations within the modeled transmission framework. The study provides important new information about how intervention tactics affect the prevalence of vector infections and the potential for further transmission.

Figure 13a – 13f compartments first show a steady and nearly linear rising trajectory in the absence of control measures, reaching significant increases by day 100. This pattern highlights the vector infection's unregulated growth, which presents a serious risk of long-term disease transmission throughout the population. The consistent increase implies that, in the absence of action, the vector infection reservoir continues to pose a hazard and promotes the pathogen's continuous spread.

On the other hand, the application of control techniques significantly modifies these dynamics. Over the course of the examined period, infected-vector populations either remained relatively steady or marginally declined, whereas the trajectories under control measures plateaued

at low levels. The effectiveness of intervention efforts in reducing the prevalence of vector infections is demonstrated by this striking discrepancy. The quick stabilization suggests that control strategies can successfully stop the cycle of transmission, lowering the likelihood of outbreaks.

The robustness of these results across different vector compartments or model parameters is demonstrated by the comparative examination across the numerous graphs. The consistency of the trend highlights how important control efforts are to vector management. Furthermore, the observed variations emphasize how crucial it is to use control methods promptly and consistently in order to maintain low levels of infection within vector populations.

7. Conclusion

In this work, we used a mathematical model to closely examine the dynamics of the co-infection of HIV/AIDS and filariasis. Atangana–Baleanu in Caputo sense fractional differential equations is used to efficiently represent combined infection. After examining the model's global and local asymptotic results, it was discovered that the model was both locally and globally asymptotically stable. The center manifold approach was used to study the bifurcation phenomenon for the model, and it was found that the model has a forward transcritical bifurcation. In order to investigate the randomness dynamics in the HIV/AIDS and filariasis co-infected model and to investigate the existence and uniqueness of the solution of the co-infected model, we integrated fractional stochastic in the form of ABC operator. In order to regulate and avoid combination infections, we developed a fractional optimal control problem with five distinct controls. We provided a detailed presentation of the mathematical conclusions necessary for the optimality system. After that, the systems with and without control are numerically solved while keeping in mind the various combinations of controls, and the results of the thorough simulations are provided. Each technique has some laminations regarding infection management, according to the simulation findings, which are addressed in depth for each situation. Lastly, we simulated the model with all controls, and the results demonstrated that utilizing the prevention and treatment controls can reduce the infection of HIV/AIDS, filariasis, and its dual infection. The current study of the dynamics of HIV/AIDS and filariasis as well as their codynamics is a new subject that has not yet been investigated mathematically.

AUTHOR CONTRIBUTIONS

All the authors have accepted responsibility for the entire content of this submitted manuscript and approved submission.

CONFLICTS OF INTERESTS

The authors declare that they have no conflicts of interests.

REFERENCES

[1] K.R. Talaat, N. Kumarasamy, S. Swaminathan, R. Gopinath, T.B. Nutman, Filarial/Human Immunodeficiency Virus Coinfection in Urban Southern India, Am. J. Trop. Med. Hyg. 79 (2008), 558-560. https://doi.org/10.4269/ajtmh.2008.79.558.

[2] S. Babu, T.B. Nutman, Immunopathogenesis of Lymphatic Filarial Disease, Semin. Immunopathol. 34 (2012), 847–861. https://doi.org/10.1007/s00281-012-0346-4.

[3] World Health Organization, Lymphatic Filariasis, 2024. https://www.who.int/news-room/fact-sheets/detail/lymphatic-filariasis.

[4] J.O. Gyapong, M. Gyapong, D.B. Evans, M.K. Aikins, S. Adjei, The Economic Burden of Lymphatic Filariasis in Northern Ghana, Ann. Trop. Med. Parasitol. 90 (1996), 39–48. https://doi.org/10.1080/00034983.1996.11813024.

[5] N. Nielsen, P. Simonsen, P. Magnussen, S. Magesa, H. Friis, Cross-Sectional Relationship Between HIV, Lymphatic Filariasis and Other Parasitic Infections in Adults in Coastal Northeastern Tanzania, Trans. R. Soc. Trop. Med. Hyg. 100 (2006), 543–550. https://doi.org/10.1016/j.trstmh.2005.08.016.

[6] Z.L. Mkhize-Kwitshana, M.L.H. Mabaso, Deworming of Filariasis and Reduction of HIV Incidence, Lancet HIV 12 (2025), e315–e316. https://doi.org/10.1016/s2352-3018(25)00010-4.

[7] E. Chavura, W. Singini, R. Chidya, B.C. Mbakaya, Immunological Responses to Helminths and HIV-1 Co-Infections, Eur. Sci. J. 1 (2023), 525. https://doi.org/10.19044/esipreprint.1.2023.525.

[8] L.R. Sangaré, B.R. Herrin, G. John-Stewart, J.L. Walson, Species-Specific Treatment Effects of Helminth/HIV-1 Co-Infection: A Systematic Review and Meta-Analysis, Parasitology 138 (2011), 1546–1558. https://doi.org/10.1017/s0031182011000357.

[9] T. Tafatatha, M. Taegtmeyer, B. Ngwira, A. Phiri, M. Kondowe, et al., Human Immunodeficiency Virus, Antiretroviral Therapy and Markers of Lymphatic Filariasis Infection: A Cross-Sectional Study in Rural Northern Malawi, PLOS Neglected Trop. Dis. 9 (2015), e0003825. https://doi.org/10.1371/journal.pntd.0003825.

[10] N. Nielsen, P. Bloch, P. Simonsen, Lymphatic Filariasis-Specific Immune Responses in Relation to Lymphoedema Grade and Infection Status. II. Humoral Responses, Trans. R. Soc. Trop. Med. Hyg. 96 (2002), 453–458. https://doi.org/10.1016/s0035-9203(02)90392-5.

[11] A.R. Carvalho, C.M. Pinto, D. Baleanu, HIV/HCV Coinfection Model: A Fractional-Order Perspective for the Effect of the HIV Viral Load, Adv. Differ. Equ. 2018 (2018), 2. https://doi.org/10.1186/s13662-017-1456-z.

[12] R. Zarin, A. Khan, P. Kumar, U.W. Humphries, Fractional-Order Dynamics of Chagas-HIV Epidemic Model with Different Fractional Operators, AIMS Math. 7 (2022), 18897–18924. https://doi.org/10.3934/math.20221041.

[13] , Mathematical Analysis of a Model for HIV-Malaria Co-Infection, Math. Biosci. Eng. 6 (2009), 333–362. https://doi.org/10.3934/mbe.2009.6.333.

[14] E. Bonyah, Y. Yuan, S. Mangal, Fractional Stochastic Modelling of Dengue Fever: The Social Awareness Perspective, Sci. Afr. 22 (2023), e01966. https://doi.org/10.1016/j.sciaf.2023.e01966.

[15] S. Y. Tchoumi, M. L. Diagne, H. Rwezaura, J. M. Tchuenche, Malaria and covid-19 co-dynamics: A mathematical model and optimal control, Applied Mathematical Modelling 99 (2021) 294–327.

[16] K. O. Okosun, O. D. Makinde, A co-infection model of malaria and cholera diseases with optimal control, Mathematical Biosciences 258 (2014) 19–32.

[17] E. Bonyah, A Fractional Dynamics of a Potato Disease Model, Commun. Math. Biol. Neurosci. 2022 (2022), 88. https://doi.org/10.28919/cmbn/7599.

[18] M.F. Farayola, S. Shafie, F.M. Siam, I. Khan, Mathematical Modeling of Radiotherapy Cancer Treatment Using Caputo Fractional Derivative, Comput. Methods Programs Biomed. 188 (2020), 105306. https://doi.org/10.1016/j.cmpb.2019.105306.

[19] D. Baleanu, A. Jajarmi, H. Mohammadi, S. Rezapour, A New Study on the Mathematical Modelling of Human Liver with Caputo–Fabrizio Fractional Derivative, Chaos Solitons Fractals 134 (2020), 109705. https://doi.org/10.1016/j.chaos.2020.109705.

[20] A.I. Abioye, O.J. Peter, H.A. Ogunseye, F.A. Oguntolu, T.A. Ayoola, et al., A Fractional-Order Mathematical Model for Malaria and COVID-19 Co-Infection Dynamics, Healthc. Anal. 4 (2023), 100210. https://doi.org/10.1016/j.health.2023.100210.

[21] A. Carvalho, C.M.A. Pinto, A Delay Fractional Order Model for the Co-Infection of Malaria and HIV/AIDS, Int. J. Dyn. Control. 5 (2016), 168–186. https://doi.org/10.1007/s40435-016-0224-3.

[22] H. Alrabaiah, M.u. Rahman, I. Mahariq, S. Bushnaq, M. Arfan, Fractional Order Analysis of HBV and HCV Co-Infection under ABC Derivative, Fractals 30 (2021), 2240036. https://doi.org/10.1142/s0218348x22400369.

[23] S. Siegmund, C. Nowak, J. Diblik, A Generalized Picard-Lindelöf Theorem, Electron. J. Qual. Theory Differ. Equ. 28 (2016), 1–8. https://doi.org/10.14232/ejqtde.2016.1.28.

[24] C. Castillo-Chavez, B. Song, Dynamical Models of Tuberculosis and Their Applications, Math. Biosci. Eng. 1 (2004), 361–404. https://doi.org/10.3934/mbe.2004.1.361.

[25] S. Lenhart, J.T. Workman, Optimal Control Applied to Biological Models, Chapman and Hall/CRC, 2007. https://doi.org/10.1201/9781420011418.